Electronic and Optical Properties of Si-Ge-Sn alloys

by

Hermann Azemtsa Donfack

A Dissertation Presented in Partial Fulfillment
of the Requirements for the Degree
Doctor of Philosophy

Approved October 2011 by the
Graduate Supervisory Committee:

Mark Van Schilfgaarde, Co-Chair
John Dow, Co-Chair
Fernando Ponce
Barry Ritchie
Ralph Chamberlin

ARIZONA STATE UNIVERSITY

December 2011

ABSTRACT

In this thesis a new method based on the Tight-Binding Linear Muffin Tin Orbital (TB-LMTO) formalism and the Quasiparticle Self-consistent GW (QSGW) approximation is proposed. The method is capable of generating accurate electronic bands structure of large supercells necessary to model alloys structures. The strategy consist in building simple and small hamiltonian from linear Muffin-tin-orbitals (LMTO). Parameters in this hamiltonian are then used to fit the difference in QSGW self-energies and LDA exchange-correlation potentials. The parameter are assumed to transfer to new environments — a procedure we check carefully by comparing our predicted band to QSGW bands for small supercells.

The method possess both the accuracy of the QSGW approximation, (which is the most reliable way to determine energy bands accurately, and yet too expensive for the large supercells required here), and the efficiency of the TB-LMTO method.

The accurate and highly efficient hamiltonian is used to predict the electronic and optical transitions of $Si_{1-x}Ge_x$ and $Ge_{1-x}Sn_x$ alloys and $Sn_xSi_yGe_{1-x-y}$ alloys. The goal is to engineered direct band gap material compatible with the silicon technology. The results obtained are compared to available experimental data.

To my parents

ACKNOWLEDGEMENTS

I was privileged to have as advisor Professor Mark van Schilfgaarde, who introduced me to the wonderful field of Electronic Structure calculations. Thank you for teaching me so much, I am deeply grateful.

I wish to thank Professor John D. Dow for his advices and his constant support and encouragements throughout my graduate work.

I would like to also thank all the members of my supervisory committee, Professor Fernando Ponce, Professor Barry Ritchie and Professor Ralph Chamberlin. I particularly wish to thank Professor José Menéndez forhis availability and most importantly his ability to convey excitement for this project.

I benefited greatly from the lectures and the interaction with the following faculty from the ASU Physics Department, Prof. Otto Sankey, Prof. Kevin Schmidt, Prof. John Shumway, Prof Andrei Belitsky, Prof. Mike Treacy and Prof. John Page.

Thank you Dr Vijay D'Costa and Dr Scott Menor for sharing your expertise and time when needed.

I am grateful to the Department of Physics and to the School of Engineering of Matter, Transportation and Energy of Arizona State University for their financial Assistantship.

Finally, I would not have carry this project to term without the moral support of all my family and friends. Thank you all.

TABLE OF CONTENTS

LIST OF TABLES

LIST OF FIGURES

Chapter 1

Introduction

1.1 Motivation and Background

Semiconductors are a very important class of material and are present in virtually all electric devices, for example transistors, solar cells and various opto-electronic devices. All these applications exploit the existence in these material of an energy band-gap which is the difference between the minimal-energy state in the conduction band and the maximal-energy state in the valence band. When the minimal-state and the maximal-state occurs at the same **k**-vector in the Brillouin zone, the gap is said to be *direct*, otherwise the gap is *indirect*. For small gap, electrons can gain enough energy by absorbing photons and move from the valence bands to the conduction bands.

Processes involving direct transition are generally more efficient, yet two of the most important semiconductors Si and Ge have indirect gaps. It was predicted by Jenkins and Dow [32] that mixing Sn which is semi-metal (band-gap = -0.4 eV) with Ge would produce a direct gap alloy. However, since the process of engineering band-gaps by alloying is not trivial especially when the material involved are not lattice-matched, growing single crystal material necessary for devices remain a challenge. Recently, using Chemical Vapor Decomposition (CVD) and molecular precursors, single crystalline samples of $Ge_{1-x}Sn_x$ and $Ge_{1-x-y}Si_xSn_y$ were successfully grown by the Kouvetakis Group [12]. They were able to grow $Ge_{1-x}Sn_x$ alloys with up to 20% Sn. Before their work, many other groups attempted to grow alloys of Si-Ge-Sn, but succeeded only in making polycrystalline or amorphous structures [25, 48]. Optical characterization of SiGeSn revealed that direct band gap can be achieved in these alloys[16, 15, 25]

The challenges present on the experimental side are carried to the theoretical side as well. Indeed, for the same reason alloys are hard to grow, they are also hard to simulate

Table 1.1: Lattice parameter for Si, Ge and Sn, the mismatch in Si-Ge is 4% compared to 16% for Si-Sn and 13% for Ge-Sn

Elements	a_{lat}(a.u.)	$a_{lat}(\AA)$
Si	10.26	5.43
Ge	10.67	5.65
α-Sn	12.25	6.48

reliably with traditional alloy calculation schemes. If Jenkins and Dow did predict that the existence of a concentration at which GeSn alloys became direct-gap material, they however overestimated the amount of Sn needed. Their prediction of concentration of 20% was twice of the experimental values of 11%. The reason for the discrepancies was the fact that the method used to model the alloy, the Virtual Crystal Approximation (VCA) is more suitable for closely matched such as Si_xGe_{1-x}. Since this work, many theoretical calculations of these alloys have been made using Density Functional Theory [56, 42, 11].

The challenges of *ab-initio* modeling of alloys are two-fold: first a suitable representation of the alloys that take into account the chemical as well as the structural disorder. Second the *ab-initio* calculation must be capable of handling large systems and also be free of the well-known band-gap problem of the Density Functional Theory [22] for meaningful comparison to experiment. Our goal is to develop a band theory method capable of generating accurate electronic bands structures of large supercells (necessary to model alloy structures). The bands generated will be used to predict various electronic and optical properties of the alloys. For the representation of our alloys, we use the Special Quasi-Random Structure (SQS) which are the small supercell mimicking random alloys.

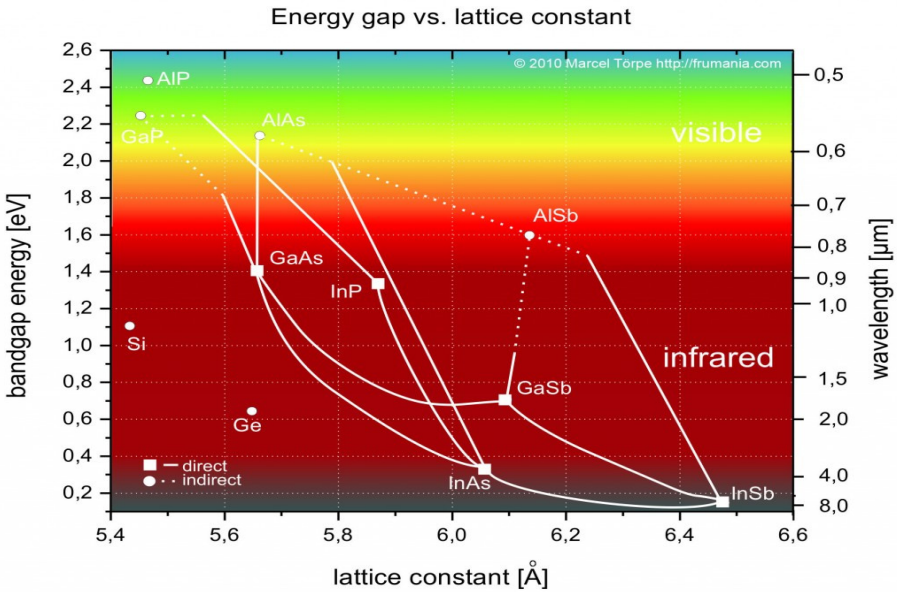

Figure 1.1: Plot of the band gap vs. lattice parameter for various semiconductors. Sn (absent from this plot) would lie near the InSb. Highly-mismatch SiSn and GeSn are hard to grow

1.2 Dissertation outline

In Chapter 2, we will review the many body problem of electrons and discuss the density functional theory in details. We will also discuss the band gap problem and briefly present the QSGW approximation.

In Chapter 3, We discuss the computational method used to solve the Schrödinger equation, in particular we review the Tight-Binding Linear Muffin-Tin-Orbitals (TB-LMTO) hamiltonian in the Atomic Sphere Approximation (ASA). In Chapter 4, we describe our the QSGW calculations of the bulk material Si, Ge and Sn are used to adjust the the parameter of the TB-LMTO hamiltonian. We end the chapter with a discussion of the transferability.

In Chapter 5, we review the optical properties of semiconductors, and establish the link between optical properties and the electronic band structures. We compare the measured dielectric function and the one calculated with our new hamiltonian.

In Chapter 6, we use our newly developed scheme to investigate the effect of alloying on band gaps and optical spectra of Si-Ge-Sn alloys. The Chapter 7, we summarize our results for the bulk material as well the alloys.

Chapter 2

The Many Body electron problem

The aim of this chapter is to provide a background of the many body electron problem. In section 2.1, we set up the Hamiltonian of the problem and introduce the notations we will be using throughout the chapter. In this section, we also discuss the Born-Oppenheimer Approximation (BOA) and the independent electron approximation. In section 2.2 a discussion of the Hartree-Fock approximation method as well as the important notion of correlation is given. Section 2.3 is the most relevant to our study and deals with the Density Functional Theory (DFT) and the Local Density Approximation (LDA). We end the chapter with a review of the Quasiparticle Self-Consistent GW (QSGW) approximation.

The topic of electronic structure has been covered in great details in many standard textbooks. Our review follows references: [6, 20, 41].

2.1 Schrödinger equation for interacting electrons and nuclei

This section covers the basic problem of the electronic structure of solids. We follow the presentation and notation of Richard Martin's *Electronic Structure* [41].

Our model solid state system consist of points nuclei of mass M and atomic number Z_I at position $\mathbf{R_I}$ as well as electrons of mass m at positions $\mathbf{r_i}$.

The Hamiltonian of such a system is given by

$$\begin{aligned} \hat{H} &= -\frac{\hbar^2}{2m}\sum_i \nabla_i^2 + \frac{1}{2}\sum_{i\neq j}\frac{e^2}{|\mathbf{r}_i-\mathbf{r}_j|} + \sum_{i,I}\frac{Z_I e^2}{|\mathbf{r_i}-\mathbf{R}_I|} \\ &- \frac{\hbar^2}{2M_I}\sum_I \nabla_I^2 + \frac{1}{2}\sum_{I\neq J}\frac{Z_I Z_J e^2}{|\mathbf{R_I}-\mathbf{R}_J|} \end{aligned} \tag{2.1}$$

The first term is kinetic energy of the electrons, the second, the electron-electron repulsion, and the third term the electron-nuclear attraction. The last two terms are re-

spectively the kinetic energy of the nuclei and the inter-nuclear repulsion. Because of the presence of the third term, the Hamiltonian is not separable into a purely electronic hamiltonian and a purely electronic hamiltonian. However, the mass of the electrons m is small compared to the mass of the nuclei M, so a perturbation series can be defined in terms of the small parameter $m/M \sim 1/1836$. If we set the nuclei mass to infinity, the first term in kinetic energy can be ignored. In doing so, we imply that the electrons move faster and react instantaneously to the motion of the nuclei. This is the **Born-Oppenheimer Approximation (BOA)**, and is in general valid, provided we are not explicitly concerned with electron-phonon interactions. We also treat the inter-nuclei interaction as a constant contribution to the electronic total energy. These approximations leave us with *electronic many-body problem*

In Hartree units $\hbar = m = e = 4\pi/\varepsilon_0 = 1$, the electronic Hamiltonian is written as

$$\hat{H} = \hat{T} + \hat{V}_{\text{int}} + \hat{V}_{\text{ext}} + E_{II} \tag{2.2}$$

where $\hat{T}$ is the kinetic energy of the electron, $\hat{V}_{\text{ext}}$ is external potential acting on the electrons due to the nuclei

$$\hat{V}_{\text{ext}} = \sum_{i,I} \frac{Z_I}{|\mathbf{r}_i - \mathbf{R}_I|}, \tag{2.3}$$

$\hat{V}_{\text{int}}$ is the many-body electron-electron interaction,

$$\hat{V}_{\text{int}} = \frac{1}{2} \sum_{i \neq j} \frac{1}{|\mathbf{r}_i - \mathbf{r}_j|} \tag{2.4}$$

and E_{II} the classical nuclei-nuclei interaction.

The fundamental equation for a non-relativistic quantum system of electrons is the time-dependent Schrödinger equation

$$i\hbar \frac{\partial \Psi(\mathbf{r}_1, \mathbf{r}_2, ..., \mathbf{r}_N; t)}{\partial t} = \hat{H} \Psi(\mathbf{r}_1, \mathbf{r}_2, ..., \mathbf{r}_N; t) \tag{2.5}$$

$\Psi(\mathbf{r}_1, \mathbf{r}_2, ..., \mathbf{r}_N; t)$ represents the many-body wave function for the system of electrons with coordinates $\mathbf{r}_1, \mathbf{r}_2, ...\mathbf{r}_N$. Since our hamiltonian is time-independent, the wave functions have the form $\Psi(\{\mathbf{r}_i\}; t) = \Psi(\{\mathbf{r}_i\}) e^{-iEt/\hbar}$. Substituting $\Psi(\{\mathbf{r}_i\}; t)$ into Eq. (2.5)

yields the time-independent Schrödinger equation

$$\hat{H}\Psi(\mathbf{r}_1,\mathbf{r}_2,...,\mathbf{r}_N) = E\Psi(\mathbf{r}_1,\mathbf{r}_2,...,\mathbf{r}_N) \tag{2.6}$$

where E the total energy of the system and is a physical observable of the operator $\hat{H}$ and as such is given the expectation value

$$E = \frac{\langle\Psi|\hat{H}|\Psi\rangle}{\langle\Psi|\Psi\rangle} = \langle\hat{H}\rangle = \langle\hat{T}\rangle + \langle\hat{V}_{\text{int}}\rangle + \int d^3r\, V_{\text{ext}}(\mathbf{r})n(\mathbf{r}) + E_{II}. \tag{2.7}$$

Another important physical observable is the particle density $n(\mathbf{r})$. It is expectation value of the *density operator* $\hat{n}(\mathbf{r}) = \delta(\mathbf{r}-\mathbf{r}')$.

$$n(\mathbf{r}) = \frac{\langle\Psi|\hat{n}(\mathbf{r})|\Psi\rangle}{\langle\Psi|\Psi\rangle} = N\frac{\int\Psi(\mathbf{r},\mathbf{r}_2,...,\mathbf{r}_N)\Psi^*(\mathbf{r},\mathbf{r}_2,...,\mathbf{r}_N)d^3r_2...d^3r_N}{\int\Psi(\mathbf{r}_1,\mathbf{r}_2,...,\mathbf{r}_N)\Psi^*(\mathbf{r}_1,\mathbf{r}_2,...,\mathbf{r}_N)d^3r_1d^3r_2...d^3r_N}. \tag{2.8}$$

Despite the simplification brought about by the BOA, we are still left with a complicated interacting many-body problem in a form partial differential equation of $3N$ variables. The complication stem from the fact that the electronic hamiltonian cannot be written as a sum of single electrons terms because of the presence of the electron-electron interaction term

$$V_{\text{int}} = V_{\text{ee}} = \frac{1}{2}\sum_{i\neq j}\frac{1}{|\mathbf{r}_i-\mathbf{r}_j|}. \tag{2.9}$$

This term implies that the motion of electrons are correlated. However, we can still assume that there exist an *effective potential* V_{eff} such that

$$V_{\text{int}} = V_{\text{ee}} = \frac{1}{2}\sum_{i\neq j}\frac{1}{|\mathbf{r}_i-\mathbf{r}_j|} = \sum_i v^i_{\text{eff}}(\mathrm{r}_i). \tag{2.10}$$

That is, we treat the electrons in our solids, as if they each moved independently, but in some effective, *mean-field*, due to the presence of other electrons. The above assumption of the existence of such *quasiparticles* convert our many-body problem into a set of independent one-body problem. This is the *independent electron approximation*. The tricky part is building V_{eff} that it computationally tractable, and yet still embodies the correlated nature of the electronic motion. The two most popular theory containing

this idea are the Hartree-Fock (HF) approximation and DFT and will be discussed in the sections below.

We will also discuss a many-body perturbation method, the GW approximation (GWA) that starts with the independent-particle wave functions and determine the energy dependent self-energy $\Sigma = iGW$ that is analog to $v^i_{\text{eff}}(r_i)$. We leave out other method such as the Quantum Monte Carlo methods which do not start with the independent-particle approximation.

2.2 Hartree-Fock Approximation

In this section, we derive the Hartee-Fock equation. We will start with Hartree method and show how improvement on the Hartree wave functions will the idea of exchange and correlation.

Hartree approximation

The strategy in the Hartree-like theories [20] is to look for separable solutions of the form

$$\Psi_m(\mathbf{r}_1, \mathbf{r}_2, ..., \mathbf{r}_N) \approx \psi_1(\mathbf{r}_1)\psi_2(\mathbf{r}_2)...\psi_N(\mathbf{r}_N) \tag{2.11}$$

representing the best approximation of the true wave function of $\hat{H}$, in the sense that they satisfy the variational principle

$$E_0 \leq \frac{\langle\Psi|\hat{H}|\Psi\rangle}{\langle\Psi|\Psi\rangle}. \tag{2.12}$$

where E_0 is the true system ground state energy. Accounting for the spins degree of freedom, the Hartree wave function has the form

$$\Phi(\mathbf{r}_1\sigma_1, \mathbf{r}_2\sigma_2, ..., \mathbf{r}_N\sigma_N) \approx \phi_1(\mathbf{r}_1\sigma_1)\phi_2(\mathbf{r}_2\sigma_2)...\phi_N(\mathbf{r}_N\sigma_N) \tag{2.13}$$

where $\phi_i(\mathbf{r}_i\sigma_i)$ is the product of the spatial and spinor part $\phi_i(\mathbf{r}_i\sigma_i) = {\psi_i}^{\sigma}(\mathbf{r}_i)\alpha(\sigma_i)$

The one-electron state $\phi_1(\mathbf{r}_i\sigma_i)$ must be orthogonal to each other since they are the

eigenstate of the one-particle hamiltonian: we have

$$\langle {\psi_i}^{\sigma}(\mathbf{r}_i)\alpha(\sigma)|{\psi_j}^{\sigma'}(\mathbf{r}_i)\alpha(\sigma')\rangle = \delta_{ij}\delta_{\sigma\sigma'} \tag{2.14}$$

Hartree-Fock Approximation

A close inspection of the Hartree approximation reveals one major shortcoming, the wave function is not *antisymmetry* under particle exchange $\mathbf{r}_i\sigma_i \rightleftharpoons \mathbf{r}_j\sigma_j$, since the electrons are indistinguishable from one another.

An attempt to fix the above failings were introduced by Fock and Slater[46] in what is called the Hartree-Fock-Slater method (HF). They constructed a wave function in the form of a Slater determinant

$$\Phi(\mathbf{r}_i\sigma_i,\mathbf{r}_i\sigma_i,...,\mathbf{r}_N\sigma_N) = \frac{1}{\sqrt{N!}}\begin{vmatrix} \phi_1(\mathbf{r}_1\sigma_1) & \phi_1(\mathbf{r}_2\sigma_2) & \phi_1(\mathbf{r}_3\sigma_3) & \cdots \\ \phi_2(\mathbf{r}_1\sigma_1) & \phi_2(\mathbf{r}_2\sigma_2) & \phi_2(\mathbf{r}_3\sigma_3) & \cdots \\ \phi_3(\mathbf{r}_1\sigma_1) & \phi_3(\mathbf{r}_2\sigma_2) & \phi_3(\mathbf{r}_3\sigma_3) & \cdots \\ . & . & . & \cdots \\ . & . & . & \cdots \end{vmatrix} \tag{2.15}$$

where the orbital have the separable form $\phi_i(\mathbf{r}_i\sigma_i) = \psi_i(\mathbf{r}_i)\alpha(\sigma_i)$.

The Pauli exclusion principle is satisfied since the determinant is zero if two orbitals are identical (ie no two electrons are allowed two be on the same state). Also because single permutation of any two rows, changes the sign of the determinant, the antisymmetry condition is satisfied.

It can be shown that the anti-symmetrization causes the electrons motion to be correlated, in fact the joint probability $n(\mathbf{r},\sigma;\mathbf{r}',\sigma')$ of finding electrons of spin σ at position $\mathbf{r}$ and of spin σ' at position $\mathbf{r}'$ is more than the product of individual probabilities $n(\mathbf{r},\sigma)$ and $n(\mathbf{r}',\sigma')$:

$$\begin{aligned} n^{\mathrm{HF}}(\mathbf{r},\sigma;\mathbf{r}',\sigma') &= n(\mathbf{r},\sigma)n\mathbf{r}',\sigma') + \Delta n_x(\mathbf{r},\sigma;\mathbf{r}',\sigma') \\ &= n(\mathbf{r},\sigma)n\mathbf{r}',\sigma') - \delta_{\sigma\sigma'}\left|\sum_i \psi^{\sigma *}(\mathbf{r})\psi^{\sigma *}(\mathbf{r}')\right|^2 \end{aligned} \tag{2.16}$$

The last term gives a measure of the correlation; and is zero in the Hartree approximation. By examining Eq. (2.16), we see that $\Delta n_x(\mathbf{r},\sigma;\mathbf{r}',\sigma') = 0$ when $\sigma \neq \sigma'$ that is, there is no correlation between particles of different spin. Also, when $\sigma = \sigma'$, $\Delta n(\mathbf{r},\sigma;\mathbf{r}',\sigma') < 0$ implying electrons with same spin avoid each other and further more if at the same time $\mathbf{r} = \mathbf{r}'$, then $n^{\mathrm{HF}}(\mathbf{r},\sigma;\mathbf{r}',\sigma') = 0$. No electron can have same spin and same position. These are evidence of the presence of correlation in the Hartree-Fock theory.

Hartee-Fock equation

It can be shown that the Hartree-Fock total energy is given by

$$\begin{aligned} E = \langle\Psi|\hat{H}|\Psi\rangle &= \sum_{i,\sigma}\int d\mathbf{r}\,\psi_i^{\sigma *}(\mathbf{r})\left[\frac{-\hbar^2}{2m}\nabla^2 + V_{\mathrm{ext}}(\mathbf{r})\right]\psi_i^{\sigma *}(\mathbf{r}) + E_{II} \\ &+ \frac{1}{2}\sum_{ij,\sigma_i\sigma_j}\int d\mathbf{r}d\mathbf{r}'\,\psi_i^{\sigma_i{}^*}(\mathbf{r})\psi_j^{\sigma_j{}^*}(\mathbf{r}')\frac{e^2}{|\mathbf{r}-\mathbf{r}'|}\psi_i^{\sigma_i}(\mathbf{r})\psi_j^{\sigma_j}(\mathbf{r}') \quad (2.17) \\ &- \frac{1}{2}\sum_{ij,\sigma}\int d\mathbf{r}d\mathbf{r}'\,\psi_i^{\sigma}(\mathbf{r})\psi_j^{\sigma}(\mathbf{r}')\frac{e^2}{|\mathbf{r}-\mathbf{r}'|}\psi_i^{\sigma}(\mathbf{r})\psi_j^{\sigma}(\mathbf{r}') \end{aligned}$$

The last two terms are the Hartree energy E_H and the exchange energy E_x. They can be re-expressed as,

$$\begin{aligned} E_H &= \frac{1}{2}\sum_{ij,\sigma_i\sigma_j}\int d\mathbf{r}d\mathbf{r}'\,\psi_i^{\sigma_i{}^*}(\mathbf{r})\psi_j^{\sigma_j{}^*}(\mathbf{r}')\frac{e^2}{|\mathbf{r}-\mathbf{r}'|}\psi_i^{\sigma_i}(\mathbf{r})\psi_j^{\sigma_j}(\mathbf{r}') \\ &= \frac{1}{2}\int d\mathbf{r}d\mathbf{r}'\,n(\mathbf{r})\frac{e^2}{|\mathbf{r}-\mathbf{r}'|}n(\mathbf{r}') \quad (2.18) \end{aligned}$$

$$E_{\mathrm{x}} = -\frac{1}{2}\sum_{ij,\sigma}\int d\mathbf{r}d\mathbf{r}'\,\psi_i^{\sigma}(\mathbf{r})\psi_j^{\sigma}(\mathbf{r}')\frac{e^2}{|\mathbf{r}-\mathbf{r}'|}\psi_i^{\sigma}(\mathbf{r})\psi_j^{\sigma}(\mathbf{r}'). \quad (2.19)$$

We have used the $n = \sum_{i,\sigma_i}\psi_i^{\sigma_i *}(\mathbf{r})\psi_i^{\sigma_i *}(\mathbf{r})$

If we now demand that the determinantal wave-function be chosen so as to minimize variationally, the total energy in Eq. (2.17), we arrive at the HF equation,

$$\left[\frac{-\hbar^2}{2m}\nabla^2 + V_{\mathrm{ext}}(\mathbf{r}) + V_{\mathrm{eff}}^{i\sigma}(\mathbf{r})\right]\psi_i^{\sigma}(\mathbf{r}) = \varepsilon_i^{\sigma}\psi_i^{\sigma}(\mathbf{r}) \quad (2.20)$$

where $V_{\text{eff}}^{i\sigma}(\mathbf{r}) = V_{\text{ext}}(\mathbf{r}) + V_H(\mathbf{r}) + V_{i\sigma}^{x}(\mathbf{r})$ and the Hartree potential V_{H} and exchange potential $V_{i\sigma}^{x}$ are respectively given by

$$V_{\text{H}}(\mathbf{r}) = \int d\mathbf{r}' n(\mathbf{r}') \frac{e^2}{|\mathbf{r}-\mathbf{r}'|} \tag{2.21}$$

$$V_{\text{x}}(\mathbf{r}) = -\left[\sum_j \int d\mathbf{r}' \psi_j^{\sigma *}(\mathbf{r}) \psi_i^{\sigma}(\mathbf{r}') \frac{e^2}{|\mathbf{r}-\mathbf{r}'|}\right] \frac{\psi_j^{\sigma}(\mathbf{r})}{\psi_i^{\sigma}(\mathbf{r})}. \tag{2.22}$$

Upon close observation of the expression (2.22), we see that the Hartee-Fock exchange potential is both orbital dependent, and non-local. This means that the Hartree-Fock one-body effective potential does contain element of the true many-body problem. The Hartree-Fock method is known to predict reasonable the properties of atoms and molecules, but is quite poor for solids, for example the Hartree-Fock Approximation predicts a silicon band gap of 0.5 eV, compared to the experimental value 1.17 eV. In addition, the method is difficult to implement because of the presence of the non-local term in 2.20.

2.3 Density Functional Theory

In this section, we review the DFT, and derive the important Kohn-Sham equation and its local density approximation (LDA). We also examine the interpretation of the DFT-LDA eigenvalue.

Hohenberg-Kohn theorems

The main idea in the density functional theory is to recast the many-body problem in terms of the particle density instead of the many-body wave functions as it is done in the HF approximation. The theory is based on two fundamental theorems [27]

Theorem 2.3.1 *For a system of interacting particles in an external potential $V_{ext}(\mathbf{r})$, the potential $V_{ext}(\mathbf{r})$ is determined uniquely except for a constant, by the ground state particle density $n_0(\mathbf{r})$.*

Theorem 2.3.2 *A universal functional for the energy $E[n]$ in terms of the density $n(\mathbf{r})$ can be defined, valid for any external potential $V_{ext}(\mathbf{r})$. For any particular $V_{ext}(\mathbf{r})$, the exact ground state energy of the system is the global minimum value of this functional, and the density $n(\mathbf{r})$ that minimizes the functional is the ground state density $n_0(\mathbf{r})$.*

Applying theorem (2.3.1) and (2.3.2) to the many-body electronic hamiltonian, Eq. (2.2),

$$\hat{H} = \hat{T} + \hat{V}_{\text{int}} + \hat{V}_{\text{ext}} + E_{II} \tag{2.23}$$

we have the Hohenberg-Kohn energy as functional of the density $n(\mathbf{r})$

$$E_{HK} \quad = \quad T[n] + E_{\text{int}}[n] + \int d\mathbf{r} n(\mathbf{r}) V_{\text{ext}}(\mathbf{r}) + E_{II} \tag{2.24}$$

with $T[n]$ and E_{int} universal functional of $n(\mathbf{r})$. Furthermore if $n(\mathbf{r})$ is the ground state density, E_{HK} is the energy of the ground state.

It is important at this point to make the following two remarks: first the HK theorems only refer to ground state properties and do not mention excited states. In principle, since $n(\mathbf{r})$ determines V_{ext} and hence the entire hamiltonian, the excited states are correctly built in. However, the functionals are only evaluated near the global minimum (ground state) far away from saddle points associated with excited states.

Second, the HK theorems only prove the existence of a unique functional $E[n]$ of the density, but the exact form of $E[n]$ remains unknown. The next section tries to address this last issue.

The Kohn-Sham Equation

Kohn and Sham formalism [34] transforms the original many-electron interacting system into an auxiliary non-interacting system with the same number of electrons. The result is an independent particle Schrödinger similar to the Hartree-Fock Approximation.

The ground state of the auxiliary system has one electron each in of the N orbitals $\psi_i^\sigma(\mathbf{r}$ with lowest eigenvalue ε_i^σ. We recall the electron density is given by

$$n(\mathbf{r}) = \sum_{i\sigma}^{N} |\psi_i^\sigma(\mathbf{r})|^2 \tag{2.25}$$

and the non-interacting kinetic energy $T_S$is given by

$$T_s = -\frac{1}{2}\sum_{i\sigma}^{N} \langle \psi_i^\sigma | \nabla^2 | \psi_i^\sigma \rangle. \tag{2.26}$$

If the coulomb interaction, E_{H} in terms of the electronic density is

$$E_{\mathrm{H}} = \frac{1}{2}\int d\mathbf{r} d\mathbf{r}' \frac{n(\mathbf{r})n(\mathbf{r}')}{|\mathbf{r}-\mathbf{r}'|}, \tag{2.27}$$

and the exact Kohn-Sham total energy is

$$E_{\mathrm{KS}} \quad = \quad T_s[n] + E_{\mathrm{H}}[n] + E_{\mathrm{ex}}[n] + \int d\mathbf{r} n(\mathbf{r}) V_{\mathrm{ext}} + E_{II} \tag{2.28}$$

The term $E_{\mathrm{xc}}[n]$ contains the many-body effect but its exact form is not known except via the relation

$$E_{\mathrm{xc}} = T[n] - T_s[n] + E_{\mathrm{int}}[n] - E_{\mathrm{H}}[n] \tag{2.29}$$

obtained by comparing Eqs. (2.24) and (2.28). In practice approximation are made about the functional form of $E_{\mathrm{xc}}[n]$, the most popular are the LDA (see next section) and generalized gradient approximation (GGA).

Assuming $E_{\mathrm{xc}}[n]$ given, the Kohn-Sham equation is obtained by minimizing Eq. (2.28) with respect to the constraint $n(\mathbf{r}) = \sum_{i\sigma}^{N} |\psi_i^\sigma(\mathbf{r})|^2$

$$\left[\frac{1}{2}\nabla^2 + V_{\mathrm{eff}}^\sigma(\mathbf{r})\right] \psi_i^\sigma(\mathbf{r}) = \varepsilon_i^\sigma \psi_i^\sigma(\mathbf{r}) \tag{2.30}$$

where

$$V_{\mathrm{eff}}^\sigma(\mathbf{r}) = V_{\mathrm{ext}}^\sigma(\mathbf{r}) + V_{\mathrm{H}}(\mathbf{r}) + V_{\mathrm{xc}}^\sigma(\mathbf{r}) \tag{2.31}$$

with

$$V_{\mathrm{xc}}^\sigma(\mathbf{r}) \equiv \frac{\delta E_{\mathrm{xc}}[n]}{\delta n(\mathbf{r})} = \frac{\delta}{\delta n(\mathbf{r})}\int d\mathbf{r} n(\mathbf{r}) \varepsilon_{\mathrm{xc}}([n];(\mathbf{r})) \tag{2.32}$$

Again Eq. (2.30) can be solved self-consistently if V_{xc} is known.

The Local Density Approximation (LDA)

The most popular exchange and correlation functional is the local density approximation. It assumes $E_{\rm xc}$ has the form

$$E_{xc}^{\rm LDA} = \int d\mathbf{r} n(\mathbf{r}) \varepsilon_{\rm xc}([n];(\mathbf{r})) \equiv \int d\mathbf{r} n(\mathbf{r}) \varepsilon_{\rm xc}(n(\mathbf{r})) \tag{2.33}$$

where $\varepsilon_{\rm xc}(n(\mathbf{r})$ is the local exchange correlation energy density of an homogeneous electron gas (HEG) with density $n(\mathbf{r})$ and are known exactly based on calculations on HEG system. The exchange and correlation potential is

$$V_{\rm xc}^{\sigma}(\mathbf{r}) \equiv \frac{\delta E_{\rm xc}[n]}{\delta n(\mathbf{r})} = \varepsilon_{\rm xc}(n(\mathbf{r})) + n(\mathbf{r}) \frac{d}{dn} \varepsilon_{\rm xc}(n(\mathbf{r})). \tag{2.34}$$

By construction, the DFT-LDA is exact in the limit of uniform density, so properties derived from the DFT-LDA will be more accurate for system which can be closely approximated by a uniform density, and inaccurate for system with strong symmetric densities.

The limitation of the DFT-LDA: Band gap problem

The grounds state properties (electronic density, total energy, bulk modulus and various elastic coefficients) are successfully predicted by the DFT-LDA. However, the excited state properties are not so well described. The most obvious example is the band gaps of semiconductors which are consistently underestimated. The silicon band gap in LDA is 0.5 eV compared to the experimental value of 1.17 eV. LDA predict Ge to be a metal (0 gap) yet Ge is semiconductor with band gap of 0.65 eV at room temperature. In order to understand the origin of these discrepancies, we have to return to the derivation of DFT.

First, the electron density is truly non-local contrary to the assumption of the LDA. Second, whereas the true meaning of the total energy and electron density is built in

the DFT, nothing guarantees the Kohn-Sham eigenvalues are physical. They were introduced as lagrange multipliers in the KS variational principle and so cannot automatically be interpreted as the true electronic energies. In fact, it has been proved that ([44, 22]) that even if the exact functional of the exchange and correlation was known, the KS energies will still not be equal to the quasiparticles excitation energies. Nevertheless the Kohn-Sham band energies are close to quasiparticle excitation energies and can be considered as a zero order approximation to the true quasiparticle energies.

Various methods have been proposed to improve the accuracy of the excitation energies. These methods can be classified into two categories: the method based on improving the functional form of the exchange and correlation energy and other methods based on many-body perturbation theory. We discussed the second category in the next section. An example in the first category is the generalized gradient approximation (GGA) ([55]) in which the gradient of the density n, ∇n is added to the LDA exchange and correlation potential. This method improves the total energy but does not affect the excited-states energies. Another common method, the LDA+U ([37]) tries to improve the LDA eigenvalues by introducing empirical orbital (d-orbital) dependent energy term U to the LDA potential. This scheme properly positions the localized d and f energy levels but does little to affect the band gap. The methods in the second category that actually improve the band gap are the Self-Interaction correction (SIC) and the Optimized Effective Potential (OEP) method. The gap though improved, are overestimated. A brief discussion of these methods is found in the review by Aryasetiawan and Gunnarson ([5]).

Other methods such as the Many-body perturbation theory can be built around the Kohn-sham hamiltonian; we discuss them in the next section.

2.4 Many-body Methods: GW approximation

In order study electron excited state and excitation spectra, we need to go beyond-DFT as we have indicated in the previous section. The method is best understood when

presented from the Green's function formalism. We will follow the presentation of Louie and Cohen[38].

Green's Function Formalism

We recall that the for a single particle Green's function for interacting many-electron system of Eq. (2.5) is given by

$$G(\mathbf{r},\mathbf{r}';\tau) \quad = \quad -i\langle 0|T\hat{\psi}(\mathbf{r},\tau)\hat{\psi}(\mathbf{r},0)|0\rangle \tag{2.35}$$

where $\hat{\psi}$ is the electron field operator, T the time order operator and $|0\rangle$ is the many electron ground state. Eq. (2.35) represent the amplitude of finding a particle at $\mathbf{r}$ a time τ if one was created in $\mathbf{r}'$ at time t=0.

From the many-body hamiltonian $H = \hat{T} + \hat{V}_{\text{ext}} + \hat{V}_{\text{int}} = H_0 + V_{\text{int}}$, we have

$$(\hbar\omega - H_0 - V_{\text{H}})G(\mathbf{r},\mathbf{r}';\omega) - \int \Sigma_{\text{xc}}(\mathbf{r},\mathbf{r}'',\omega)G(\mathbf{r}'',\mathbf{r}';\omega) = \delta(\mathbf{r},\mathbf{r}') \tag{2.36}$$

where $\Sigma_{\text{xc}}(\mathbf{r},\mathbf{r}',\omega)$ is the self-energy. Re-expressing green's function as

$$G(\mathbf{r},\mathbf{r}',\omega) = \sum_{n\mathbf{k}} \frac{\psi_{n\mathbf{k}}(\mathbf{r})\psi^*_{n\mathbf{k}}(\mathbf{r}')}{\omega - E_{n\mathbf{k}} \pm i\delta} \tag{2.37}$$

we obtain the quasiparticle *Dyson's equation*

$$\left[\frac{-\hbar^2}{2m}\nabla^2 + V_{\text{ext}}(\mathbf{r}) + V_{\text{H}}(\mathbf{r})\right]\psi_{n\mathbf{k}}(\mathbf{r}) + \int d^3\mathbf{r}'\Sigma_{\text{xc}}(\mathbf{r},\mathbf{r}',\omega)\psi_{n\mathbf{k}}(\mathbf{r}') = E_{n\mathbf{k}}\psi_i(\mathbf{r}) \tag{2.38}$$

where $\psi_{n\mathbf{k}}$ the eigenfunctions of the Dyson's equation and $E_{n\mathbf{k}}$ the eigenvalues also corresponding to the pole of $G(\omega)$.

Eq. (2.38) is similar in form to Eq. (2.30) with the difference that the $V_{\text{xc}}(\mathbf{r},\mathbf{r}')$ is replaced by the self-energy $\Sigma_{\text{xc}}(\mathbf{r},\mathbf{r}',\omega)$. Compared to $V_{\text{xc}}(\mathbf{r},\mathbf{r}')$, the self-energy is non-local, energy dependent and contains all the effects of exchange and correlation. $\Sigma_{\text{xc}}(\mathbf{r},\mathbf{r}',\omega)$ is not hermitian, therefore, $E_{n\mathbf{k}}$ has a real part corresponding the quasiparticle energies and an imaginary part linked to their lifetime assumed to be long enough

to warrant comparison with experiments. Constructing $\Sigma_{\rm xc}(\mathbf{r},\mathbf{r}',\omega)$ is complicated, and approximations have to be made. The most common is the GW approximation(GWA), first introduced by Hedin [26].

The GW approximation (GWA)

The GWA is a perturbative approach to the many-body problem around a one body hamiltonian $H_0 = \frac{\nabla^2}{2} + V_{\rm eff}(\mathbf{r},\mathbf{r}')$; usually the H_0 is the DFT-LDA hamiltonian. The method consists of expanding the self-energy in terms of the green's function G^0 and the screened coulomb interaction W, keeping only the first term of the expansion. In this approximation, the self-energy is given as

$$\Sigma(\mathbf{r},\mathbf{r}',\omega) \approx \frac{i}{2\pi}\int d\omega' G^0(\mathbf{r},\mathbf{r}',\omega-\omega')W(\mathbf{r},\mathbf{r}',\omega)e^{-i\delta\omega'}. \tag{2.39}$$

where G_0 is obtained from the eigenvalues ε_i and eigenfunctions Ψ_i of H_0:

$$G^0(\mathbf{r},\mathbf{r}',\omega) = \sum_i \frac{\Psi_i(\mathbf{r})\Psi_i^*(\mathbf{r}')}{\omega-\varepsilon_i \pm i\delta} \tag{2.40}$$

and W calculated in the random phase approximation (RPA)

$$W = \varepsilon^{-1}v = (1-v\Pi)^{-1}v; \tag{2.41}$$

where ε is the dielectric function, $\Pi = -iG^0 \times G^0$ is the proper polarization function and $v(\mathbf{r},\mathbf{r}') = \frac{1}{|\mathbf{r}-\mathbf{r}'|}$ the bare coulomb interaction.
If we define a GW-one effective potential $V_{\rm eff}^{\rm GW}$ as

$$V_{\rm eff}^{\rm GW}(\omega) = V_{\rm eff} + \Sigma(\omega) = V_{\rm H} + V_{\rm ext} + \Sigma(\omega). \tag{2.42}$$

we can think of GWA as a perturbative correction $\Delta V_{\rm eff}^{\rm GW}(\omega)$ to one-particle potential $V_{\rm eff}$ that is

$$\Delta V(\omega) = V_{\rm eff}^{\rm GW}(\omega) - V_{\rm eff} \tag{2.43}$$

As mentioned earlier, the starting hamiltonian is in most cases the LDA hamiltonian, $H_0 = H^{\mathrm{LDA}}$ and in this case,

$$E_{n\mathbf{k}} = \varepsilon_{n\mathbf{k}} + Z_{n\mathbf{k}} \langle \Psi_{n\mathbf{k}} | \Sigma(\mathbf{r}, \mathbf{r}', \varepsilon_{n\mathbf{k}}) - V_{\mathrm{xc}}^{\mathrm{LDA}}(\mathbf{r}) | \Psi_{n\mathbf{k}} \rangle \tag{2.44}$$

where $Z_{n\mathbf{k}}$ is the quasiparticle renormalization factor

$$Z_{n\mathbf{k}} = 1 - \langle \Psi_{n\mathbf{k}} | \frac{\partial}{\partial \omega} \Sigma(\mathbf{r}, \mathbf{r}', \varepsilon_{n\mathbf{k}}) | \Psi_{n\mathbf{k}} \rangle \tag{2.45}$$

This approach to the GWA is often called the *one-shot-GW*, and was first implemented by Hybertsen and Louie [28]. The energy bands of the one-shot GWA are a large improvement compared to the LDA bands. However, the energy values often depend on the starting hamiltonian H_0, and different H_0 lead to different GW energies. This suggest *self-consistency* is needed.

Many self-consistent GW (SC-GW) scheme have been implemented in the past. Aryasetiawan *et al* [4] used one such scheme to study the energy bands structure of NiO and Luo *et al* [40] for the bands structure of ZnS and ZnSe. In these two cases, the eigenvalues were calculated self-constistently, without varying the *one-shot* wave function. Later, Kotani and van Schilfgaarde *et al* [50, 35] implemented the more rigorous *Quasiparticle Self-consistent GW (QSGW)* method. We present a summary of the important steps of the QSGW method.

Quasiparticle-self-consistent GW approxiamtion

The QSGW approach to self-consistency is to find the best H_0 (or V_{eff}) from which QP energies are derived. This is done by looping between V_{eff} and $V_{\mathrm{GW}}(\omega)$ until the difference $\Delta V(\omega)$ is minimum. For the minimization step, Kotani *et al* [35] introduced a norm M given by

$$M[V_{\mathrm{eff}}] = Tr[\Delta V \delta(\omega - H_0) \Delta V^{\dagger}] + Tr[\Delta V^{\dagger} \delta(\omega - H_0) \Delta V] \tag{2.46}$$

where the trace is taken over $\mathbf{r}$ and ω. They showed this norm was minimized by choosing V_{xc} in $V_{\text{eff}} = V_{\text{ext}} + V_{\text{H}} + V_{\text{xc}}$ as

$$V_{\text{xc}} = \frac{1}{2}\sum_{ij} |\psi_i\rangle \left\{ \text{Re}\left[\Sigma(\varepsilon_i)\right]_{ij} + \text{Re}\left[\Sigma(\varepsilon_j)\right]_{ij} \right\} \langle\psi_j| \tag{2.47}$$

With the new V_{xc}, a new H_0 is constructed and the GWA step repeated to generate a new Σ. The process is repeated until convergence is reached. Achieving self-consistency in this manner insures that QSGW approximation converges in both the eigenvalues and eigenfunctions, in contrast to the SC-GW.

The excited states energies (and thus the values of the band gap) are in better agreement with experiments for many semiconductors as it is shown in Figs. (2.1) [50]. This success comes at a huge cost in computational time; this is the case because apart from the calculation of the polarization function which is an expensive step in the GWA, the QSGW requires both the diagonal Σ_{ii} and the off-diagonal element Σ_{ji} of the self energy matrix.

In this thesis, we only use the QSGW method for bulk Si, Ge and Sn which only have two atoms in their unit cell. We will perform QSGW calculations on few 8-atoms structures. The main use of our QSGW results will be to provide us with the accurate energies band needed for our fits.

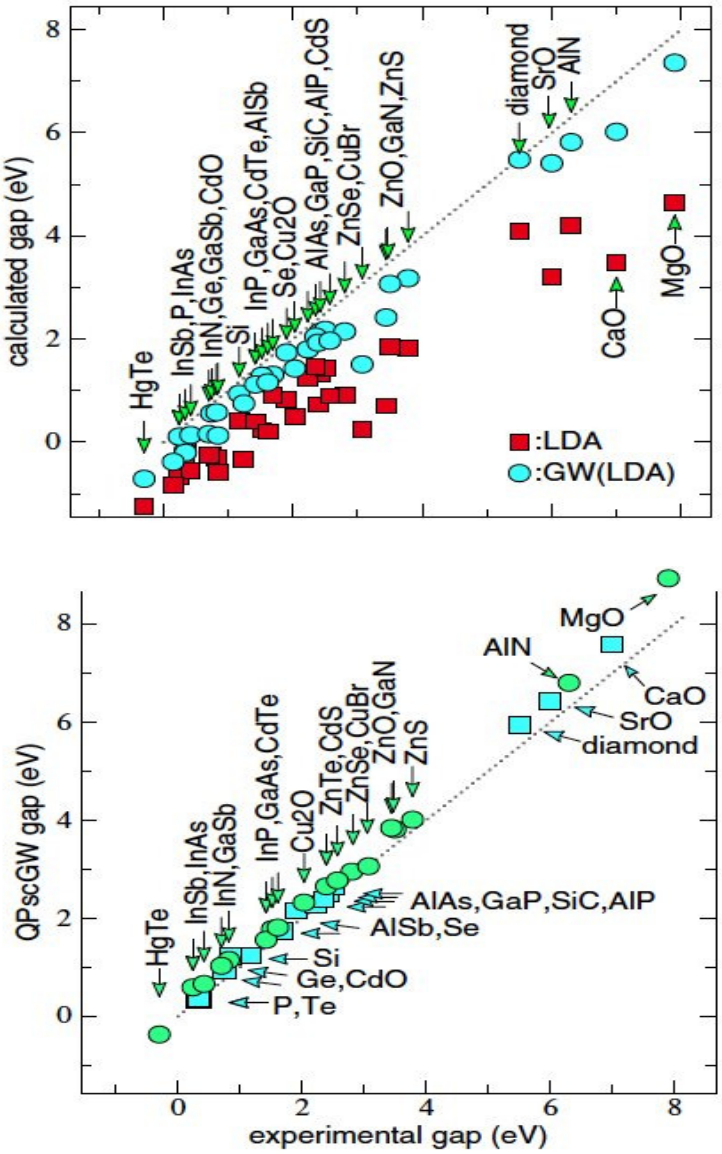

Figure 2.1: Fundamental gaps of sp compounds from LDA (squares) and $G^{LDA}W^{LDA}$ (circles) in top panel, and from QSGW, in bottom panel. For QSGW data, zinc-blende compounds with direct $\Gamma - \Gamma$ transitions are shown as circles; All other gaps are shown as squares from [50]

Chapter 3

Solutions of the one-electron problem

The purpose of this chapter is to solve the one-electron Kohn-Sham equation derived in the previous chapter:

$$\left[-\frac{\nabla^2}{2}+V(\mathbf{r})\right]\psi_i(\mathbf{r})=\varepsilon_i\psi_i(\mathbf{r}) \tag{3.1}$$

We use the Tight-Binding Linear Muffin-Tin orbitals (TB-LMTO) method in the Atomic Sphere Approximation (ASA). This method was developed by O. K. Andersen[2, 3] over many years. The method is built around the classical multiple scattering method of Korringa, Kohn and Rostoker (KKR) [29, 33]. The basis used are minimal, short ranged, thus particularly suitable for the supercell calculations we are interested in. We first review the derivation of the TB-LMTO method, then we apply the method and modification thereof to the calculation of band structures of Si, Ge and Sn.

3.1 From Multiple scattering theory to TB-LMTO

The TB-LMTO method has been discussed in greater detail in many monograms and texts. The following presentation is based on the textbook of G.P. Das[14]. First we present the MTO in the context of the KKR-MTO, next we introduced the Atomic Sphere Approximation (ASA) before discussing the concept of screening and linearization of the MTO eigenvalue problem.

We can imagine the effective potential experienced by electrons in condensed-matter being the result of overlapping individual atomic potentials as atoms come closer and

closer to form a solids. This potential can be approximated by MT potential

$$V(\mathbf{r}) = \sum_R V_R(|\mathbf{r}\text{-}\mathbf{R}|) + V_{\mathrm{MT}} \tag{3.2}$$

here R is sum over all atomic sites. $V(\mathbf{r})$ is spherically symmetric within the MT radius S_R and constant in the interstitial region.

Muffin tin orbital and the tail cancellation theorem

The solution of Eq. (3.1) for a single MT, has the form

$$\chi_{RL}(\varepsilon,\kappa,r_R) = \hat{Y}_L(\hat{r}_R) \begin{cases} \phi_{Rl}(\varepsilon,r_R) & r_R \le s_R \\ n_l(\kappa r_R) - \cot(\eta_{Rl}(\varepsilon,\kappa)) j_l(\kappa r_R) & r_R \ge s_R \end{cases} \tag{3.3}$$

where $r_R = |r-R|$ and $L = \{lm\}$. $\phi_{Rl}(\varepsilon,r_R)$ is the solution of the radial schrödinger equation inside the MT and the solution in the interstitial is a linear combination of the Neumann function $n_l(\kappa r_R)$ and the Bessel function $j_l(\kappa r_R)$. $\kappa^2 = \varepsilon - V_{\mathrm{MT}}$ is the kinetic energy in the interstitial region. Finally $\eta_{Rl}(\varepsilon,\kappa)$ is the "phase shift" of the l-partial wave which is determined by matching the inside and interstitial solution at the MT-radius s_r. Put mathematically,

$$\cot(\eta_{Rl}(\varepsilon,\kappa)) = \frac{W[\phi_{Rl}(\varepsilon,r_R), n_l(\kappa r_R)]}{W[\phi_{Rl}(\varepsilon,\kappa), j_l(\kappa r_R)]} \tag{3.4}$$

with the $W[]$ the traditional wronskian. In order to avoid divergence of the solution in the interstitial when $\kappa \le 0$, we add to the general solution $\cot(\eta_{Rl} j_l(\kappa r_R)$ and obtain the so-called *muffin-tin orbital*

$$\chi_{RL}(\varepsilon,\kappa,r_R) = \hat{Y}_L(\hat{r}_R) \begin{cases} \phi_{Rl}(\varepsilon,r_R) + \cot(\eta_{Rl}(\varepsilon,\kappa)) j_l(\kappa r_R) & r_R \le s_R \\ n_l(\kappa r_R) & r_R \ge s_R \end{cases} \tag{3.5}$$

The "tail" of the MTO centered at R $n_l(\kappa r_R)$ may be expanded into spherical harmonics about another sites R' as

$$n_l(\kappa r_R) \sum_{L'} j'_L(\kappa r_{R'}) B_{RL,R'L'}(\kappa) \tag{3.6}$$

The expansion coefficient is the KKR structure matrix $B_{RL,R'L'}$.

For the full crystal, the solution of Eq. (3.1) may now be expressed as a linear combination of MTO:

$$\psi(\varepsilon, r) = \sum_{RL} \chi_{RL}(\varepsilon, \kappa, r_R) c_{RL} \tag{3.7}$$

on the condition that inside any MT R' and for any angular momentum L', the contribution from neighboring tails must cancel the $\cot(\eta_{Rl}(\varepsilon,\kappa))\, j_l(\kappa r_R)$-term from their own MTO. This lead to the KKR *tail-cancellation condition*

$$\sum_{RL} [B_{R'L',RL}(\kappa) + \cot(\eta_{Rl}(\varepsilon,\kappa))\delta_{RR'}\delta_{LL'}] c_{RL}(\varepsilon) = 0. \tag{3.8}$$

Eq. 3.8 is a system of linear equation and the zero of its secular determinant.

$$det|B(\kappa) + \cot(\eta(\varepsilon,\kappa))| = 0. \tag{3.9}$$

gives the energies and the wave function coefficient c_{RL} This last step essentially concludes the solution of Eq. (3.1) using KKR-MTO.

Few remarks can be made about the KKR-MTO solutions just outlined:

- The basis, and hence the structure constants $B(\kappa)$ are strongly energy dependent and long-ranged. It will be useful to screened the basis thus reducing their range.
- The secular determinant is nonlinear and finding its zeros is a cumbersome task; a linear secular determinant will make the problem more tractable.

Before introducing the concept of screening and linearization, we first discuss the Atomic Sphere Approximation; though the linearization and screening are independent of the ASA.

Atomic Sphere Approximation

The ASA consists in increasing the size of the MT sphere until the space is filled and the sum of the sphere volume equal the volume of the whole space. Doing so intro-

duces possible overlaps between neighboring spheres. Experience has shown that such overlap can be allowed as long as they remain small:

$$\frac{s_R - s_{R'} - |R - R'|}{s_R} \leq 0.3 \text{ for all } R \tag{3.10}$$

This condition is generally fulfilled for closed packed solid such as metal. For open structure such as semiconductors, artificial atom of charge $Z = 0$ must be added at well chosen symmetry point until the space is filled, while respecting the overlap criteria of Eq. (3.10).

The one consequence of invoking the ASA is that, the kinetic energy κ^2 can be conveniently set to zero. This imply that the regular solution of laplace's equations is now the radial Bessel and Hänkel functions

$$J_l^0(r) = \frac{1}{2(2l+1)} \left(\frac{r}{w}\right)^l \qquad K_l^0(r) = \left(\frac{r}{w}\right)^{-l-1}$$

where w is a scaling constant, usually set to the s_r (or s_{av} for compounds). Again, expanding the Hankel function in terms of static multipoles gives

$$K_l^0(r_R) = \sum_{L'} J_{L'}^0(r_{R'}) S_{RL,R'L'}^0. \tag{3.11}$$

The ASA-MTO is given by

$$\chi_{RL}(\varepsilon, r_R) = \hat{Y}_L(\hat{r}_R) \begin{cases} \phi_{Rl}(\varepsilon, r_R) + P_{Rl}^0(\varepsilon) \left(r_R/s_R\right)^l & r_R \leq s_R \\ \left(r_R/s_R\right)^{-l-1} & r_R \geq s_R \end{cases} \tag{3.12}$$

with the matching conditions giving the potential function

$$P_{Rl}^0(\varepsilon) = 2(2l+1) \frac{D_{Rl}(\varepsilon) + l + 1}{D_{Rl}(\varepsilon) - l} \tag{3.13}$$

Here $D_{Rl} \equiv D\{\phi(\varepsilon, s_R)\}$ ($D\{f\} = r\frac{f'(\mathbf{r})}{f(\mathbf{r})}$) is the logarithmic derivative of $\phi(\varepsilon, s_R)$ evaluated at $r_R = s_R$.

Now the *tail-cancellation* condition yields

$$\sum_{RL} [S_{R'L',RL} + P_{R'l'}^0(\varepsilon) \delta_{RR'} \delta_{LL'}] [N_{Rl}^0(\varepsilon)]^{-1} c_{RL}(\varepsilon) = 0. \tag{3.14}$$

where the normalization function $N^0_{Rl}(\varepsilon) = [(w/2)\dot{P}^0(\varepsilon)]^{1/2}$ with $\dot{P}^0_{R'l'}(\varepsilon)$ the energy derivative of the potential function. The new secular determinant

$$det|S^0_{R'L',RL} + P^0_{R'L',RL}(\varepsilon)\delta_{RR'}\delta_{LL'}| = 0. \tag{3.15}$$

is now clearly divided into a structure dependent part and potential dependent part. However two issues remain; First, the secular determinant is still non-linear. Second, the structure matrix is long-ranged and decays slowly as

$$S^0_{l'lm} = C_{ll'm}\left(\frac{d}{s}\right)^{-(l+l'+1)}. \tag{3.16}$$

where $C_{ll'm}$ represents the hopping parameter (similar to the one found in the context of the local combination of atomic orbitals (LCAO) [24]). The main reason for the slow decay is because the spherical Bessel (j_l) and the Neuman (n_l) functions have long range and are energy dependent. This leads to sites interference.

Screening formalism

In this section, we introduced the concept of screening, needed to make the structure matrix decay faster. In order to achieve localization, the multipole field at $\mathbf{R}$ is screened by surroundings it with multipoles at $\mathbf{R}'$.

We can write the envelope function extended over the whole space as

$$K^{0,\infty}_{Rl}(r_R) = K^0_{Rl}(r_R) - \sum_{L'} J^0_{L'} S^0_{RL,R'L'} + K^{0,i}_{Rl}(r_R) \tag{3.17}$$

or in matrix notation,

$$|K^{0,\infty}\rangle = |K^0\rangle - |J^0\rangle S^0 + |K^0\rangle^i \tag{3.18}$$

Here, $|K^0\rangle$ is the 'head' of the envelop centered at R' and vanishes outside the sphere, while $|J^0\rangle$ is regular solution, and vanishes outside neighboring WS cell centered at R' due to tail cancellation. Since we have adopted the ASA, we drop the interstitial

contribution $K^0\rangle^i$

In order to screen the envelope function $|K^{0,\infty}\rangle$, we introduce a new representation or a transformation characterized by the screened parameter $\alpha \equiv \alpha_{Rl}$. The screening transformation may be expressed by

$$J^{\alpha}_{Rl}(r_R) = J^0_{Rl}(r_R) - \alpha_{RL} K^0_{Rl}(r_R), \tag{3.19}$$

$$|K^{\alpha}\rangle\infty = |K^0\rangle - |J^{\alpha}\rangle S^{\alpha} = |K^0\rangle(1+\alpha S^{\alpha}) - |J^0\rangle S^{\alpha} \tag{3.20}$$

and

$$S^{\alpha} = S^0(1-\alpha S^0) \quad \text{or} \quad (S^{\alpha})^{-1} = (S^{\alpha})^{-1} - \alpha \tag{3.21}$$

In all the above equations, α is diagonal matrix with element α_{Rl}. When $\alpha_{Rl} = 0$, we recover the unscreened or 'bare' representation while $\alpha_{Rl} = \gamma_{Rl}$ is called the orthonormal representation and $\alpha = \omega_{Rl}$ the most localized TB-MTO representation $\alpha = 0$. It was found by trial and error [3] that the set of α yielding the best localization is *universal* and their values are $\alpha_s = 0.3485$, $\alpha_s = 0.05303$ and $\alpha_d = 0.0107$ for $l = 0, 1, 2$ and 0 for $l > 2$. For these values, S^{α} decays exponentially as $S^{\alpha} = A\exp(-\lambda^{\alpha}_{ll'}\frac{d}{w})$, with $d = |\mathbf{R\text{-}R'}|$.

In the new representation, the potential has the form

$$P^{\alpha}(\varepsilon) = P^0(\varepsilon)[1-\alpha P^0(\varepsilon)] \quad \text{or} \quad [P^{\alpha}(\varepsilon)]^{-1} = [P^{\alpha}(\varepsilon)]^{-1} - \alpha \tag{3.22}$$

and the normalization by $N^{\alpha}(\varepsilon) = [(s/2)\dot{P}^{\alpha}(\varepsilon)]^{1/2}$. The screened secular equation become

$$det|S^{\alpha}_{R'L',RL} + P^{\alpha}_{R'L',RL}(\varepsilon)\delta_{RR'}\delta_{LL'}| = 0. \tag{3.23}$$

Linear Muffin Tin Orbitals

Our goal is to construct energy independent LMTO. We begin by taylor-expanding the energy dependent MTO about a suitable energy $\varepsilon = E_v$

$$\phi_{Rl}(\varepsilon, r_R) = \varphi_{Rl}(\varepsilon, r_R) + (\varepsilon - E_v)\dot{\varphi}_{Rl}(\varepsilon, r_R) + \emptyset(\varepsilon - E_v)^2 \tag{3.24}$$

where $\varphi_{Rl}(r) = \phi(E_\nu, r)$ and $\dot{\varphi}_{Rl}(r) = \partial\phi(\varepsilon, r)/\partial\varepsilon|_{\varepsilon=E_\nu}$ are respectively the solutions of

$$[-\nabla^2 + V_R - E_\nu]\varphi(r) = 0 \tag{3.25}$$

$$[-\nabla^2 + V_R - E_\nu]\dot{\varphi}(r) = \varphi(r) \tag{3.26}$$

with normalization and orthogonality conditions (γ-representation)

$$\langle\varphi|\varphi\rangle = \int_0^{s_R} [\phi_{Rl}^\gamma]^2 r^2\, dr = 1 \quad \text{and} \quad \langle\varphi|\dot{\varphi}\rangle = \int_0^{s_R} [\phi_{Rl}^\gamma \dot{\phi}_{Rl}^\gamma] r^2\, dr = 0. \tag{3.27}$$

In the general representation, we have

$$\phi_{Rl}^\alpha(\varepsilon, r) = \phi_{Rl}^\gamma(\varepsilon, r)[N_{Rl}^\alpha(\varepsilon)/N_{Rl}^\alpha] \tag{3.28}$$

$$\dot{\phi}_{Rl}^\alpha(\varepsilon, r) = \dot{\phi}_{Rl}^\gamma(\varepsilon, r)[N_{Rl}^\alpha(\varepsilon)/N_{Rl}^\alpha] + \phi_{Rl}^\gamma(\varepsilon, r)[\dot{N}_{Rl}^\alpha(\varepsilon)/N_{Rl}^\alpha] \tag{3.29}$$

Noting that $\varphi_{Rl}^\alpha = \varphi_{Rl}^\gamma = \varphi_{Rl}$ at $\varepsilon = E_\nu$, the last expression takes the matrix notation

$$|\dot{\varphi}_{Rl}^\alpha\rangle = |\dot{\varphi}_{Rl}^\gamma\rangle + |\varphi_{Rl}^\gamma\rangle o^\alpha \tag{3.30}$$

with $o^\alpha = \langle\varphi|\dot{\varphi}^\alpha\rangle = \dot{N}^\alpha/N^\alpha = \ddot{P}^\alpha/2\dot{P}^\alpha$. Others orthogonality relations between $|\varphi\rangle$, $|\dot{\varphi}^\alpha\rangle$ and $|\dot{\varphi}^\gamma\rangle$ are

$$\langle\varphi|\varphi\rangle = 1 \quad \langle\varphi|\dot{\varphi}^\gamma\rangle = 0 \quad \langle\dot{\varphi}^\alpha|\dot{\varphi}^\alpha\rangle = p^\alpha = o^{\alpha^2} + p^\gamma \tag{3.31}$$

with $p_{Rl}^\alpha = \langle\dot{\varphi}_{Rl}^{\alpha^2}\rangle$. Using the above definition, we can write the energy independent LMTO in the ASA as

$$\chi_{Rl}(\varepsilon, r_R) = \varphi_{Rl}(\varepsilon, r_R) + \sum_{R'L'} \dot{\varphi}_{RL}(\varepsilon, r_{R'}) h_{R'L',RL}^\alpha \tag{3.32}$$

or in matrix notation

$$|\chi^\alpha\rangle = |\varphi^\alpha\rangle + |\dot{\varphi}^\alpha\rangle h^\alpha \tag{3.33}$$

where the matrix element of h^α are defined in such a way that $|K^\alpha\rangle\infty$ and $|J^\alpha\rangle$ are continuously connected to φ and $\dot{\varphi}$. Explicitly,

$$h^\alpha = -P^\alpha(\dot{P}^\alpha)^{-1} + (\dot{P}^\alpha)^{-1/2}S^\alpha(\dot{P}^\alpha)^{-1/2} \quad (3.34)$$

$$= (C^\alpha - E_\nu) + \sqrt{\Delta^\alpha}S^\alpha\sqrt{\Delta^\alpha} \quad (3.35)$$

The above expression has two parts, the on-site and diagonal part, $C^\alpha - E_\nu$ and the off-diagonal part $\sqrt{\Delta^\alpha}S^\alpha\sqrt{\Delta^\alpha}$. C^α is often called the *band-center parameter* and Δ^α the *band-width parameter*. They are related to potential parameter by

$$C^\alpha = E_\nu - P^\alpha(\dot{P}^\alpha)^{-1} \quad \text{and} \quad \Delta^\alpha = 1/\dot{P}^\alpha \quad (3.36)$$

In this basis, the overlap matrix and the Hamiltonian matrix are given by

$$\langle\chi^\alpha|\chi^\alpha\rangle = 1 + \langle\varphi^\alpha|\dot{\varphi}^\alpha\rangle h^\alpha + \langle\dot{\varphi}^\alpha|\varphi^\alpha\rangle h^\alpha + h^\alpha\langle\dot{\varphi}^\alpha|\dot{\varphi}^\alpha\rangle h^\alpha \quad (3.37)$$

$$\langle\chi^\alpha|H - E_\nu|\chi^\alpha\rangle = h^\alpha + h^\alpha\langle\dot{\varphi}^\alpha|\dot{\varphi}^\alpha\rangle h^\alpha + \cdots \quad (3.38)$$

In the nearly orthonormal representation ($\alpha = \gamma$), and neglecting higher order terms of h^α, we have the TB-LMTO-ASA hamiltonian

$$\langle\chi^\alpha|\chi^\alpha\rangle = 1 \quad (3.39)$$

$$\langle\chi^\alpha|H - E_\nu|\chi^\alpha\rangle = h^\alpha \quad (3.40)$$

3.2 The Full-Potential (FP)-LMTO method

We digress here to discuss a variant of the LMTO method, the Full-Potential LMT0. Because the spherical averaging of the charge density, the ASA is only suitable for determining the spectral properties. But properties related to the total energy are not reliable, yet many properties such as force and elastic coefficient are useful. In addition, in complex geometries, it is not always possible to fill the space with empty spheres without incurring large overlap. For this reason, the FP-LMTO were developed[39].

The LMTO-ASA and the FP-LMTO are similar in the sense that they all use linear MT-basis. But they differ in the way they treat the interstitial part of the potential. The ASA eliminates the interstitial by introducing empty spheres when necessary and can thus find the charge density by spherical averaging and avoid the very expensive calculation of the interstitial potential. The FP instead, treats the interstitial density and potential more explicitly. This make the FP somehow computationally more intense because the extra matrix $V_{ij} = \int_I d\mathbf{r} H*_i(r) V(r) H*_j(r)$. Here $H(r)$ represents the envelop function, more precisely the *smoothed Hankel functions* which make the calculation of the three-dimensional integral more efficient. The augmentation in the FP is also slightly different than in the standard LMTO. Because of this full treatment of the potential, the FP-LMTO is more accurate but unfortunately slower, and not amenable to the TB form. Throughout this thesis, we will still use the FP-LMTO in three ways:

- first to perform relaxation of the alloys in our supercell since FP-LMTO forces are accurate;
- second to generate the QSGW reference bands;
- lastly to verify that the choice of RMT radius in the LMT0-ASA is appropriate.

the GW calculations are done in the FP-LMTO while the supercell calculations are performed using the TB-LMTO-ASA.

3.3 Step of the TB-LMTO-ASA method

Let summarize the step we take to solve our Schrödinger equation (3.1). We seek wave functions $\psi(r)$ which are linear combination of $\sum_{RL} \chi_{RL} c_{RL}$ of the LMTO χ_{RL}. The eigenvectors c_{RL} and eigenenergies ε are found by solving the eigenvalue problem

$$\sum_{RL} (H_{R'L',RL} - \varepsilon O_{R'L',RL}) c_{RL} = 0 \tag{3.41}$$

where

$$H_{R'L',RL} = C_{RL}\delta_{R'R}\delta_{L'L} + \sqrt{\Delta_{R'L'}}S^{\gamma}_{R'L',RL}\sqrt{\Delta_{RL}} \quad (3.42)$$

$$O^{\gamma} = \delta_{R'R}\delta_{L'L} \quad (3.43)$$

$$S^{\gamma}_{R'L',RL} = [S^0(1-\gamma S^0)^{-1}]_{R'L',RL} \quad (3.44)$$

In practice, given a material, its crystal structure (FCC, BCC, SC, Diamond or Supercell), and its lattice parameter a_{lat}, the basis is set by deciding which angular momentum states $l = 0, 1$ and/or $2)$ (corresponding to *s, p* and/or *d*) for each atomic species present in a unit cell. With this information the structure matrix $S^{\gamma}_{R'L',RL}$ is determined. The next step is to used some starting spherically averaged electron density $n_R(r)$, of the energy moment $Q^{(m)}_{Rl} =,\ m = 0,1,2$ to construct the potential. The expression for the spherical averaged density is

$$n_R(r) = \frac{1}{4\pi}\sum_l [Q^{(0)}_{Rl}\varphi^2_{Rl}(r) + 2Q^{(1)}_{Rl}\varphi_{Rl}(r)\dot{\varphi}_{Rl}(r) + Q^{(2)}_{Rl}\{\dot{\varphi}^2{}_{Rl}(r) + \varphi_{Rl}(r)\ddot{\varphi}_{Rl}(r)\}] \quad (3.45)$$

with

$$Q^{(m)}_{Rl} = \int^{E_F} dE N_{Rl}(E)(E - E_{\nu,Rl})^m \quad (3.46)$$

where N_{Rl} is the projected density of state and is given by

$$N_{Rl}(E) = \sum_i \delta(\varepsilon - \varepsilon_i)\sum_{RL}|c_{RL}|^2 \quad (3.47)$$

Then by solving the radial equation around the energy of interest $E_{\nu,RL}$, one obtained the quantities φ_{Rl}, $\dot{\varphi}_{Rl}$ and $\ddot{\varphi}_{Rl}$ from which the potential parameter C_{RL} and Δ_{RL} are calculated. With the potential parameter, the hamiltonian $H_{R'L',RL}$ is constructed and diagonalized to obtain the eigenvalue and eigenvector. These eigenvectors are used to generate a new density. The cycle is repeated until convergence is reached.

3.4 LDA+Levenberg-Marquardt (LDA+LM) fit

The steps just described correspond to the standard TB-LMTO-ASA method. When the method is used within the DFT-LDA, the excited state energies are incorrect. In

this thesis we propose a **new method** for correcting the excited states energies of the DFT-LDA within the TB-LMTO method. The procedure consists in first determining self-consistently, the potential parameters C_{RL} and Δ_{RL} by following the steps outlined in the previous section. Then, using the Levenberg-Marquardt Non-Linear fitting techniques [45], we adjust these parameter until the eigenvalues of the TB-LMTO are the same as the QSGW energies. These fits are **only** done for elemental Si, Ge and Sn. The correction to the potential parameters are assumed to be transferable to the alloys structures. This last assumption is carefully tested.

This scheme is only possible because of the TB-LMTO-ASA provides a tight binding-like formulation of the DFT-LDA. In this sense, our approach is similar to the local density derived semi-empirical pseupotential method of Zunger [52]. It is different from the other semi-empirical tight binding method, based on Linear Combination of Atomic Orbitals (LCAO)[51, 30]. In TB-LCAO, the matrix elements are not evaluated explicitly but instead fitted to experiment; by contrast, our matrix elements are first obtained self-consistently within DFT-LDA before the LM fits are applied. In addition, the number of parameter to fit is large in TB-LCAO typically 20 to 40 compared to a maximum of 8 for similar systems.

Chapter 4

Electronic band structure of Si, Ge and $\alpha-$Sn

In this chapter, we apply our LDA+LM method to generate accurate band structures for bulk Si, Ge and Sn by adjusting the parameters of the TB-LMTO hamiltonian. The new parameters will be tested for transferability.

4.1 Fitting TB-LMTO bands to QSGW: case of Bulk Si, Ge, and $\alpha-$Sn

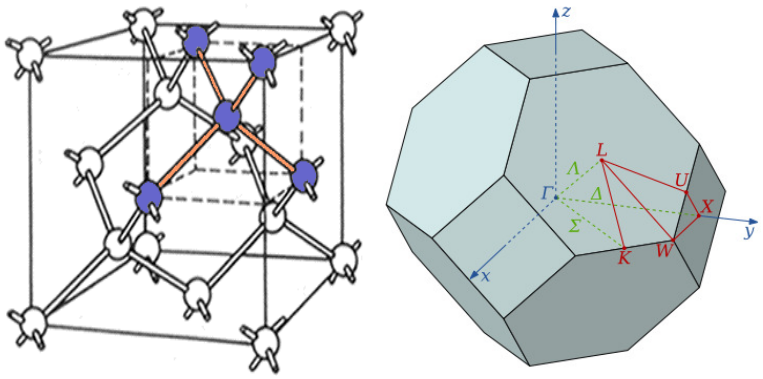

Figure 4.1: The Diamond Cell and its first Brillouin zone lattice with key symmetry point labelled

Si, Ge and ,α-Sn are all Group IV material. They are characterized by their diamond structure; an FCC structure with two atoms in the basis: one at the origin (0,0,0) and the other at (1/4, 1/4, 1/4). This gives each atom 4 nearest neighbors with which they form sp^3 tetrahedral bond as shown in Fig. 4.1.

We use for all our calculation the LMTO-ASA-V7 suite, the FP-LMTO-V7 suite and the GW-suite developed by M. van Schilfgaarde *et al.*

For all three systems, Si, Ge and Sn, our diamond unit cell contains the two atoms, plus two (extra) empty spheres(ES) necessary to fill the interstitial. In all cases, the overlap is not allowed to exceed 13.7%. The atomic configurations are for Si ([Ne]$3s^2 3p^2$), for Ge ([Ar] $4s^2 3d^{10} 4p^2$) and for Sn([Kr]$5s^2 4d^{10} 5p^2$). Therefore our basis is made in each

case of $(1\times s+3\times p+5\times d=9)*4=36-10=26$ orbitals. Here, we down-folded the 5-d-orbitals on each ES.

For each system, the first step is to obtain the QSGW reference energy bands; Next, we determined the self-consistent potential parameter of the TB-LMTO method, $\mathbf{C}_{RL}$ and Δ_{RL}. We then run the Levenberg-Marquardt fit to obtain the shifts c_{RL} and δ_{RL}. The new parameters $C_{RL}+c_{RL}$ and $\Delta_{RL}+\delta_{RL}$ give band structures that matched the QSGW bands as shown in Fig. 4.2. The agreement is excellent for the valence band as well as for the conduction bands at least up to 8 eV. The tables 4.1, 4.2 and 4.3 list the values of the potential parameters and their shifts.

Table 4.1: Si potential parameters and the shifts from GW fits (in units of Rydberg)

Elements	states	C_{RL}	c_{RL}	Δ_{RL}	δ_{RL}
		Si (alat=10.26 rmt=2.52587098)			
	s	-0.838	-0.0385	0.158	0.021
Si	p	0.115	0.018	0.131	0.025
	d	1.528	-0.004	0.141	0.001
	s	0.068	0.068	0.180	-
Es	p	1.296	0.107	0.200	-
	d	3.140	-	0.230	-

Table 4.2: Germanium potential parameters and the shifts from GW fits (in units of Rydberg)

Elements	states	C_{RL}	c_{RL}	Δ_{RL}	δ_{RL}
		Ge (alat=10.67 rmt=2.626807)			
	s	-0.951	-0.065	0.137	0.031
Ge	p	0.061	0.020	0.124	0.031
	d	1.867	-0.289	0.161	-0.020
	s	0.049	0.030	0.168	-0.020
Es	p	1.188	-0.062	0.187	-0.02
	d	2.899	-	0.214	-

Table 4.3: Tin potential parameters and the shifts from GW fits (in units of Rydberg's)

Elements	states	C_{RL}	c_{RL}	Δ_{RL}	δ_{RL}
		Sn (alat=12.25 rmt=3.015782)			
	s	-0.896	-0.052	0.104	0.026
Sn	p	-0.042	0.034	0.101	0.026
	d	1.554	-0.00	0.144	0.001
	s	-0.010	0.043	0.127	-0.025
Es	p	0.820	-0.004	0.134	-0.004
	d	2.016	-	0.144	-

4.2 Transferability

In order to test the transferability of our parameters, we used the shifts obtained for bulk Si, Ge and Sn and without any additional fit, and generate the band structures of zinc-blende (ZB) SiGe, GeSn and SiSn. The generated bands are compared to the respective QSGW bands. Fig. 4.3 shows the excellent agreement between LDA+LM bands and the QSGW. This confirms that the parameter can be reliably transferred to other environments or structures. We also calculated bands structures for few randoms alloys structures, Ge_7Sn_1 and Si_4Sn_4 all model represented by SQS-8 structures, and the ternary system $Sn_1Si_2Ge_5$ see Fig. 4.4. In all the tree cases we see that the the LDA+LM and the QSGW bands overlap. We are therefore confident that the method can be applied to our Si-Ge-Sn alloys.

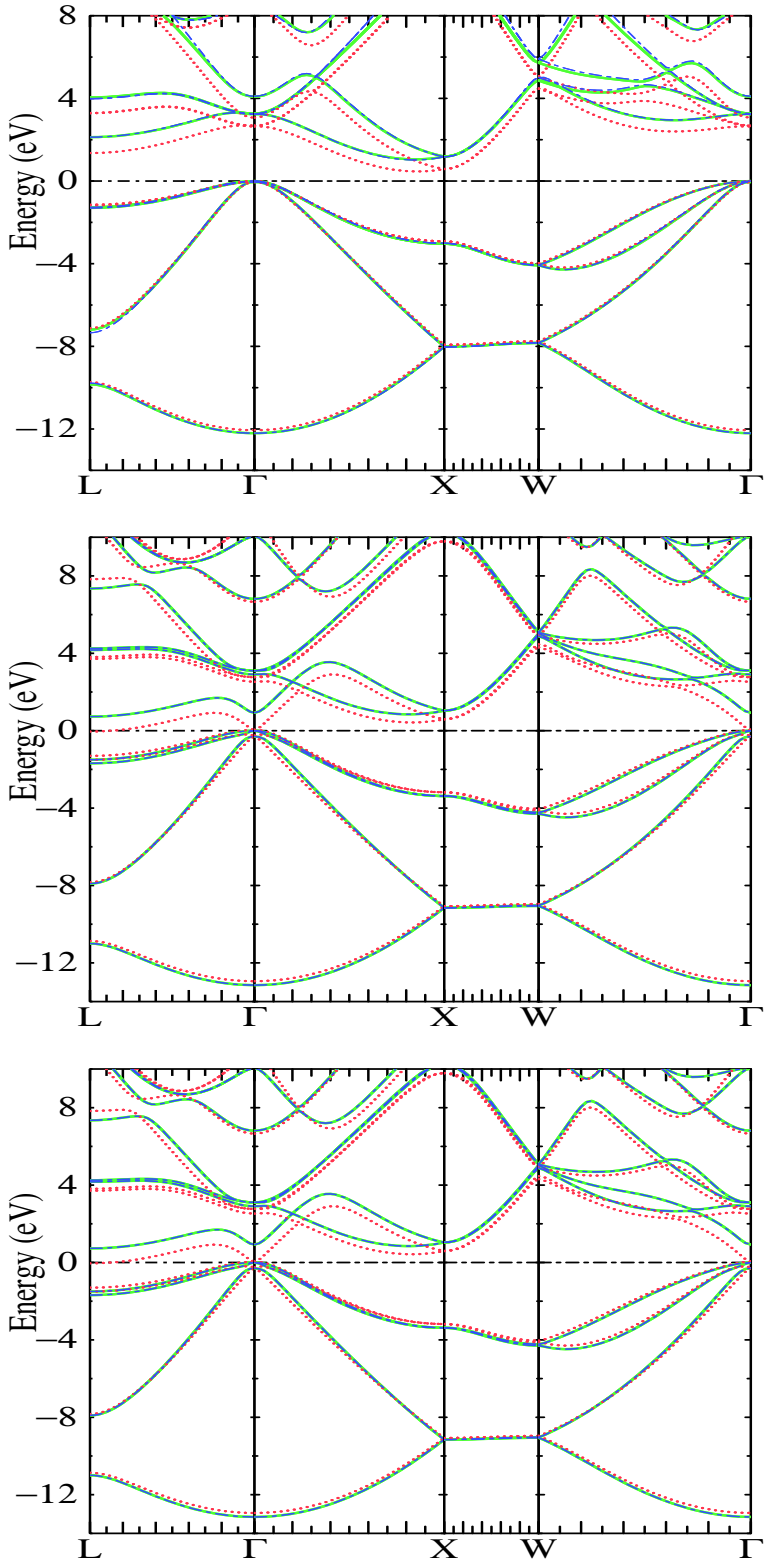

Figure 4.2: Band structure of Si(top), Ge(center), and Sn(bottom)using QSGW(solid/Green), LDA+LM(dashes/Blue) and LDA(dots/Red)

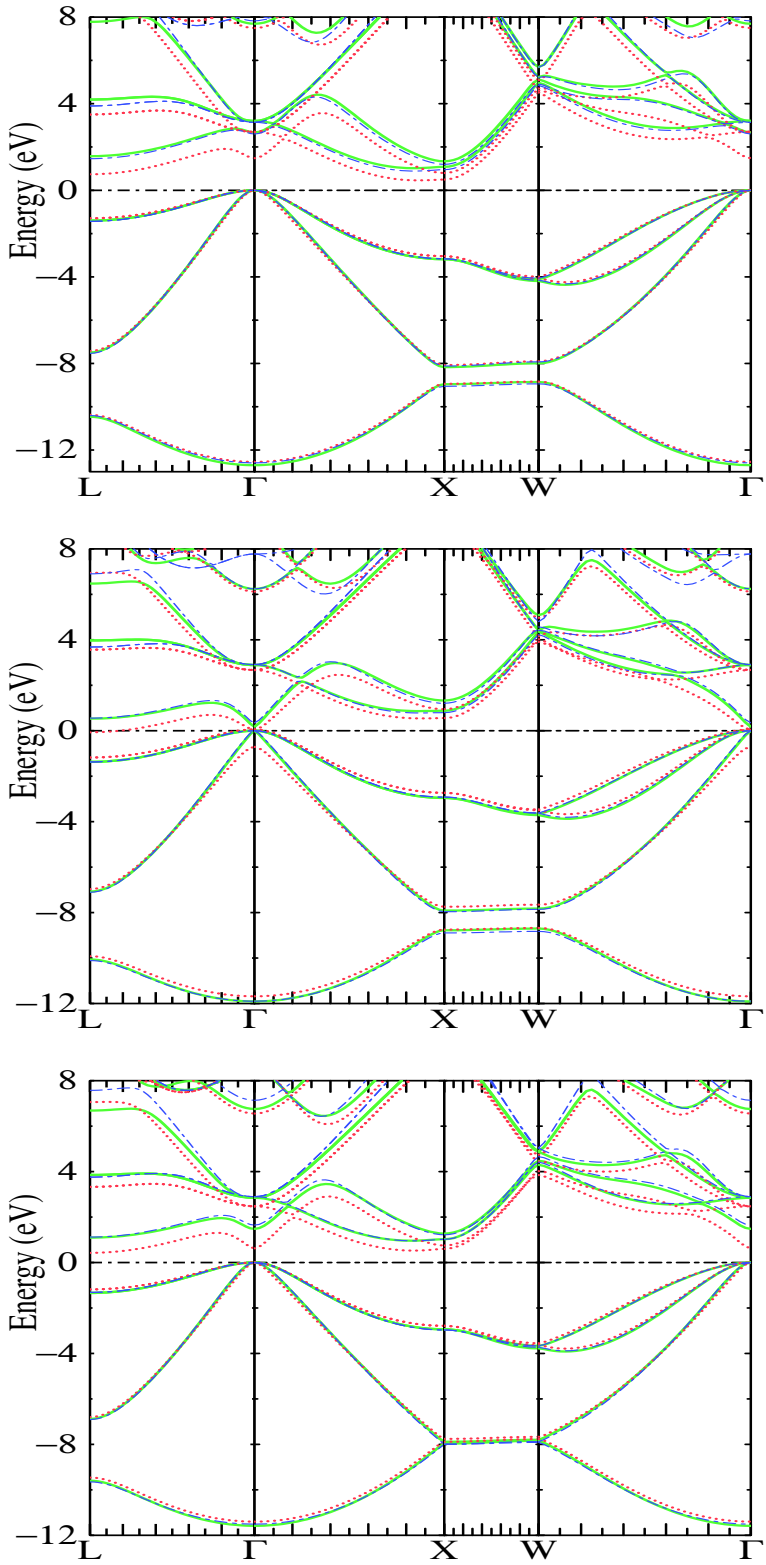

Figure 4.3: Band structure of ZB-SiGe(top), ZB-GeSn(center), and ZB-SiSn(bottom) using QSGW(solid/Green), LDA+LM(dashes/Blue) and LDA(dots/Red)

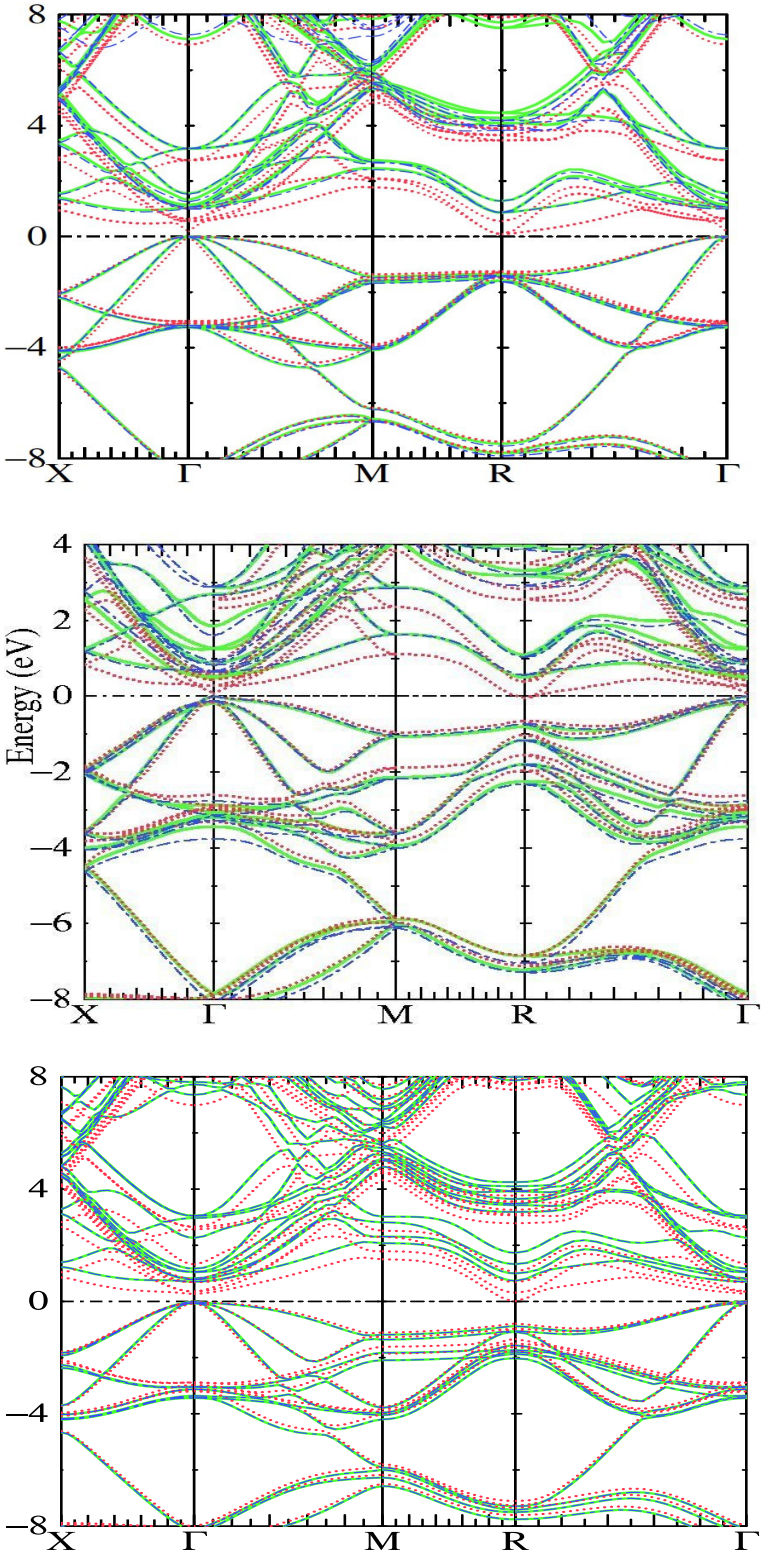

Figure 4.4: Band structure of Ge_7Sn_1(top), Si_4Sn_4(center), and $Sn_1Si_2Ge_5$(bottom) using using QSGW(solid/Green), LDA+LM(dashes/Blue) and LDA(dots/Red)

Chapter 5

Optical properties of Si, Ge and $\alpha-$ Sn

In this chapter, we derive an expression of the dielectric function of a semiconductors crystal exposed to an electromagnetic radiation, in this case visible light. The expression derived will be used together with the bands structure calculations, to generate optical spectra. Comparison with available experiment will be a further test of the capability of our new method. We recall that our focus is on determining the contribution to the dielectric function from direct interband transitions: we therefore ignore all phonon's assisted transitions as well as excitonic effects.

Optical properties of semiconductors have been discussed in the original references such as [17, 1] as well as in many standard texts [21, 57]. In section 5.1, we will present a derivation of the frequency dependent macroscopic dielectric function using semi-classical method, for this we will follow the discussion of F. Basanni *et al* [7]. In section 5.2, we use the concept of joint density-of-states to introduce the critical point used to characterize transitions. Finally in section 5.3, we show our calculated spectra for Si, Ge, Sn and GaAs.

5.1 The Dielectric Function

Macroscopic Electrodynamics

Suppose a dielectric material is subjected to an external electromagnetic plane wave represented by

$$E(r,t) = E_0 e^{i(\mathbf{q}\cdot\mathbf{r}+\omega t)} \tag{5.1}$$

where q is the wave vector and ω the frequency. The fields will induce in the material a polarization vector P given by [57]

$$P_i(\mathbf{r}',t') = \varepsilon_0 \int \chi_{ij}(|\mathbf{r}-\mathbf{r}'|),|t-t'|))E_j(\mathbf{r},t)d\mathbf{r}dt. \tag{5.2}$$

Here χ_{ij} is the electric susceptibility tensor and ε_0 the permittivity of free space. Taking the Fourier transform we have

$$P_i(\mathbf{q},\omega) = \varepsilon_0 \chi_{ij}(\mathbf{q},w))E_j(\mathbf{q},\omega) \tag{5.3}$$

Knowledge of $\chi_{ij}(\mathbf{q},w)$ in principle determines all the linear optical response of the medium, but since we are interested in a connection with experiment, we will focus on the dielectric tensor defined by

$$D_i(\mathbf{q},\omega) = \varepsilon_0 \varepsilon_{ij}(\mathbf{q},w)E_j(\mathbf{q},\omega) \tag{5.4}$$

where $\mathbf{D}(\mathbf{q},\omega)$ is the Fourier transform of the electric displacement. Recalling that $\mathbf{D} = \mathbf{E} + 4\pi\mathbf{P} = \varepsilon\mathbf{E}$, we have :

$$\varepsilon_{ij}(\mathbf{q},w)) = 1 + \chi_{ij}(\mathbf{q},w) \tag{5.5}$$

For most applications, $\varepsilon_{ij}(\mathbf{q},\omega))$ is independent of q since the wavelength of visible light is 400 nm $< \lambda <$ 800 nm and too large compared to typical lattice parameter $a_{\text{lat}} \equiv .5$ nm, thus the dielectric tensor will be only a function of ω.

Also for linear media, and cubic symmetry, the tensor ε has only three identical diagonal elements so we can now replace $\varepsilon_{ij}(\omega)$ with the scalar complex quantity $\varepsilon(\omega)$, called *dielectric function*. The dielectric function is related to the complex index of refraction N and the reflectivity R [13]:

$$\begin{aligned} \varepsilon = \varepsilon_1 + i\varepsilon_2 \qquad & N = n + i\kappa \\ \varepsilon_1 = n^2 - \kappa^2 \qquad & \varepsilon_2 = 2n\kappa \\ N^2 = \varepsilon = \varepsilon_1 + i\varepsilon_2 \quad & R = \left|\tfrac{N-1}{N+1}\right|^2 = \tfrac{(n-1)^2+\kappa^2}{(n+1)^2+\kappa^2} \end{aligned} \tag{5.6}$$

while the absorption coefficient and the average energy density in the medium are given respectively by

$$\alpha = \frac{2\kappa\omega}{c} = \frac{\omega}{nc}\varepsilon_2 \quad \text{and} \quad u = \frac{n^2}{2\pi}|E_0|2 \tag{5.7}$$

Semi-classical derivation of the dielectric function

We wish to calculate the dielectric response of a semiconductors crystal due to the electromagnetic radiation characterized Eq. (5.1) from time-dependent perturbation theory. The potential is given by $\mathbf{A}(r,t) = A_0\mathbf{e}e^{(i\mathbf{q}\cdot\mathbf{r}-\omega t)}$ so that we have $A_0 = -i\frac{c}{\omega}E_0 = -i\frac{E_0}{q}$. The electronic Hamiltonian in the presence of this field is

$$H = \frac{1}{2m}(\mathbf{p}+e\mathbf{A})^2 + V_c(\mathbf{r}) \tag{5.8}$$

where $V_c(\mathbf{r})$ is the periodic crystal potential. Under the Lorentz gauge ($\nabla\cdot\mathbf{A}=0$ and neglecting non-linear effects, the interaction part of our Hamiltonian is

$$H_{int} = \frac{e}{mc}\mathbf{A}\cdot\mathbf{p} \tag{5.9}$$

We recall that from first order perturbation theory, given an interaction $H_{int} = H_{int}e^{\mp i\omega t}$, the transition probability per unit time for an electron in state $|i\rangle$ of energy E_i to a state $|f\rangle$ of energy E_f is given by the *Fermi's golden rule*:

$$P_{i\to f} = \frac{2\pi}{\hbar}|\langle f|H_{int}|i\rangle|^2\delta(E_f - E_i \mp \hbar\omega) \tag{5.10}$$

$H_{int}e^{-i\omega t}$ induces processes in which photons with energy $\hbar\omega$ are absorbed while $H_{int}e^{+i\omega t}$ causes emission of photons with the energy $\hbar\omega$. We are interested in absorption resulting in transition from occupied valence state to empty excited state.

If our initial state is a valence band Bloch eigenstate $|v\mathbf{k}_v\rangle$ and the final, the conduction band states, $|c\mathbf{k}_c\rangle$, the matrix element of the interaction $\langle c|H_{int}|v\rangle$ of Eq. (5.9) become:

$$\langle c|H_{int}|v\rangle = \frac{e}{mc}\langle c\mathbf{k}_v|\mathbf{A}\cdot\mathbf{p}|v\mathbf{k}_v\rangle. \tag{5.11}$$

substituting $\mathbf{A}(\mathbf{r},t)$ in the above expression gives the *transition probability per unit time*

$$P_{v\to c} = \frac{2\pi}{\hbar}\left(\frac{eA_0}{mc}\right)^2|\langle c\mathbf{k}_c|e^{(i\mathbf{q}\cdot\mathbf{r})}\mathbf{e}\cdot\mathbf{p}|v\mathbf{k}_v\rangle|^2\delta(E_c - E_v - \hbar\omega) \tag{5.12}$$

Again from $\langle c\mathbf{k}_c|e^{i\mathbf{q}\cdot\mathbf{r}}\mathbf{e}\cdot\mathbf{p}|v\mathbf{k}_v\rangle$, conservation of momentum requires $\mathbf{k}_c = \mathbf{k}_v + \mathbf{q} + \mathbf{G}$ or $\mathbf{k}_c = \mathbf{k}_v + \mathbf{q}$ inside the 1st-BZ. As mentioned in the last section, for the range of frequency of interest, $\mathbf{q}$ is negligible small and the momentum conservation becomes $\mathbf{k}_c \equiv \mathbf{k}_v$. This is the so-called *dipole approximation*, and as a consequence, only vertical transitions are allowed. The probability simplifies to

$$P_{v\to c} = \frac{2\pi}{\hbar}\left(\frac{eA_0}{mc}\right)^2 |\mathbf{e}\cdot\mathbf{M_{cv}}(\mathbf{k})|^2\delta(E_c(\mathbf{k}) - E_v(\mathbf{k}) - \hbar\omega) \tag{5.13}$$

with $\mathbf{e}\cdot\mathbf{M_{cv}}(\mathbf{k}) = \langle c\mathbf{k}|\mathbf{e}\cdot\mathbf{p}|v\mathbf{k}\rangle$.

Finally, summing over all the states in the unit volume, we have the number of transition per unit time per unit volume

$$W(\omega) = \frac{2\pi}{\hbar}\left(\frac{eA_0}{mc}\right)^2 \sum_v\sum_c \int_{\mathrm{BZ}} \frac{2d\mathbf{k}}{(2\pi)^3}|\mathbf{e}\cdot M_{cv}(k)|^2\delta(E_c(\mathbf{k}) - E_v(\mathbf{k}) - \hbar\omega) \tag{5.14}$$

Connection with optical constants

The absorption coefficient mentioned in Eq. (5.7) can be given in terms of the energy absorbed per unit time per unit volume divided by the energy flux, that is

$$\alpha(\omega) = \hbar\omega\frac{W(\omega)}{u(n/c)} \tag{5.15}$$

so using from Eqs. (5.14) and (5.15), we have

$$\alpha(\omega) = \frac{4\pi e^2}{m^2 nc\omega}\sum_v\sum_c \int_{\mathrm{BZ}} \frac{2d\mathbf{k}}{(2\pi)^3}|\mathbf{e}\cdot\mathbf{M_{cv}}(\mathbf{k})|^2\delta(E_c(\mathbf{k}) - E_v(\mathbf{k}) - \hbar\omega) \tag{5.16}$$

and recalling $\alpha = \frac{\omega}{nc}\varepsilon_2$ gives finally

$$\varepsilon_2(\omega) = \frac{4\pi e^2}{m^2\omega^2}\sum_v\sum_c \int_{\mathrm{BZ}} \frac{2d\mathbf{k}}{(2\pi)^3}|\mathbf{e}\cdot\mathbf{M_{cv}}(\mathbf{k})|^2\delta(E_c(\mathbf{k}) - E_v(\mathbf{k}) - \hbar\omega) \tag{5.17}$$

This expression of the dielectric function is very useful because it provides a direct connection between the band structure obtained theoretically and the measured optical properties.

With the knowledge of the imaginary part of the dielectric function, the real part can be obtained from the *Kramer-Kronig relation*

$$\varepsilon_1(\omega) = \mathrm{Re}[\varepsilon_M] = 1 + \frac{1}{\pi} P \int_0^\infty \frac{\omega' \varepsilon_2(\omega') d\omega'}{[(E_c(\mathbf{k}) - E_v(\mathbf{k}))/\hbar]^2 - (\hbar\omega')^2} \tag{5.18}$$

Thus the knowledge of ε_2 specify completely the dielectric function as well as the complex index of refraction $N = n + ik$ and the reflectivity R using Eq. (5.6).

Also related to the Kramer-Kronig relation, are the useful *sum-rule* which can serve as a test of the accuracy of the calculated or measured response functions; some of these sum-rules are

$$\varepsilon_1(0) = 1 + \frac{2}{\pi} \int_0^\infty \frac{\varepsilon_2(\omega)}{\omega} d\omega \tag{5.19}$$

and the *f-sum rule*

$$\int_0^\infty \omega \varepsilon_2(\omega) d\omega \;\; = \;\; \frac{\pi}{2} \omega_p^2 \tag{5.20}$$

where ω_p is the electron plasma frequency given by

$$\omega_p = \left(\frac{4\pi n e^2}{m} \right)^{1/2}$$

5.2 Joint density of states and critical points

The dipole matrix elements in the expression of $\varepsilon_2(\omega)$, are usually slowly varying functions of $\mathbf{k}$ except at some symmetry points of BZ. If we assume this to be the case, we can take $\mathbf{e} \cdot \mathbf{M_{cv}}(\mathbf{k})$ outside the integral, and we see that from Eq. (5.17), much of the features (peaks) emanate from the term,

$$J_{cv}(\hbar\omega) = \int_{\mathrm{BZ}} \frac{2d\mathbf{k}}{(2\pi)^3} \delta(E_c(\mathbf{k}) - E_v(\mathbf{k}) - \hbar\omega), \tag{5.21}$$

the so-called *joint density of states* (JDOS) because it gives the combined density of a pair of states one occupied the other empty. To see the irregular form of the JDOS, using the properties of the delta-function, we write

$$J_{cv}(E) = \frac{2}{(2\pi)^3} \int_{E_c(\mathbf{k}) - E_v(\mathbf{k}) = E} \frac{dS}{|\nabla_K [E_c(\mathbf{k}) - E_v(\mathbf{k})]|}, \tag{5.22}$$

where dS represent an element of the k-space surface $E_c(\mathbf{k}) - E_v(\mathbf{k}) = E$. From this last

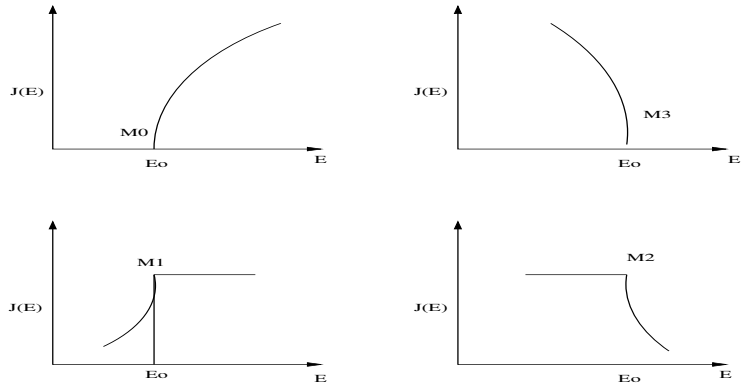

Figure 5.1: Joint density of states plotted against Energy for different critical points. M_1, M_2: saddle point; M_0: minimum point; M_3: maximum point

expression, we can see that JDOS will possess singularities where $|\nabla_K(E)| = 0$. These are called the *critical points* (CP) and the corresponding singularity in the ordinary density of states are called the *Van Hove Singularities* [49]. In 3-D, using a Taylor series about the critical point $\mathbf{k}_0$, we have

$$E_c(\mathbf{k}) - E_v(\mathbf{k}) = E_0 + \sum_{i=1}^{3} a_i(ki - k_{0i}).$$

Depending on the sign of the coefficients a_i's Van Hole distinguished 4 kinds of CP: M_0, M_1, M_2 and M_3. M_1 and M_2 are called *saddle points* while M_0 and M_3 are the *minimum and maximum point* respectively see Fig. 5.1. The CP correspond respectively to E_0, E_1, E_2 and E_3, a notation introduced by Cardona to label the important transitions in optical spectra. An example of the label is shown in Fig. 5.2.

5.3 Application: Dielectric function and JDOS for Si, Ge, Sn and GaAs

We have calculated the dielectric function $\varepsilon_2(\omega)$[1], JDOS and DOS for bulk Si, Ge, Sn and GaAs using the Optics Package (V7.4) inside the LMTO-ASA SUITE of M. van Schilfgaarde; The matrix element are calculated with our new TB-LMTO-ASA

[1] contribution from direct interband transition only

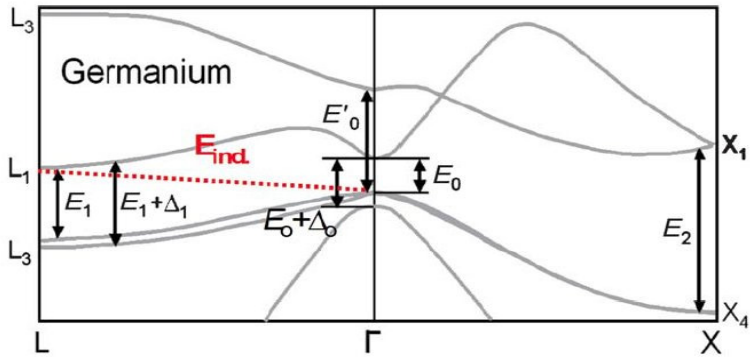

Figure 5.2: Sketch of the band structure of Germanium showing direct transition.

wave function. We used the tetrahedron method with $40 \times 40 \times 40$ k-mesh for the BZ integration. The results are shown in Figs. 5.3-5.10. The following general trends can be observed:

- The LDA+LM are shifted relative to the LDA dielectric functions while conserving the sum-rule Eq. (5.20) as we see in table 5.1.

- The LDA+LM results matches the critical peaks: E_0, E_1, E_2 and E_3 in all four systems. This agreement with experimental dielectric shows that our method can be used to interpret optical spectra from ellipsometry and photoluminescence experiments.

- The height of the E_1 peak is consistently underestimated. Other one-electron method such as the Exact Exchange (EXX) method also underestimate the height of E_1 peak [47]. It is widely accepted that including *local-field corrections*, and *excitonic effects* will improved the height of the peak, without shifting them. We also concede they are errors inerrant to the TB-LMTO-ASA

We have shown that our method can reproduce the experimental peaks of the imaginary part of the dielectric function. We also showed that by comparing ε_2 and the DOS, using the log-scale, we can determine whether the band-gap is *direct* or *indirect*.

For indirect-gap materials, the onset of the DOS occurs before the onset of the ε_2(or JDOS)[2], whereas for direct-gap materials the onset of DOS and ε_2 coincide. We can see from Fig. 5.4 and Fig. 5.6, that Ge and Si are both indirect-gap material while GaAs is clearly a direct-gap material as Fig. 5.10 confirms. Obviously, it was not necessary to compare the DOS and ε_2-lineshapes to establish the nature of the gap, the bands structure plots of the previous chapter already contained that information. However this approach will be useful when we study alloys, as the band structures of alloys, generated from supercell calculations, are hard to interpret because of band-folding. This point will be made clearer in the next chapter where we investigate the effect of allowing on the band gap and the optical spectra.

Table 5.1: Values of the f-sum rule in Eq. (5.20) in units of $\hbar^{-2}$ and for various energy cut-off.

	Ecut(Ry)	*f-sum rule ASA*	*f-sum rule ASA-FIT*
Ge	1	0.946	0.9086
	2	1.0920	1.1087
	3	1.0920	1.1087
Si	1	0.8555	0.7689
	2	1.0188	0.9469
	3	1.0188	0.9469
Sn	1	0.6598	0.6874
	2	0.7796	0.8225
	3	0.7796	0.8225
GaAs	1	0.9406	0.9289
	2	1.1121	1.1465
	3	1.1121	1.1465

[2]we remind the reader that only contribution from direct interband transitions are included in our calculations of ε_2 and of the JDOS

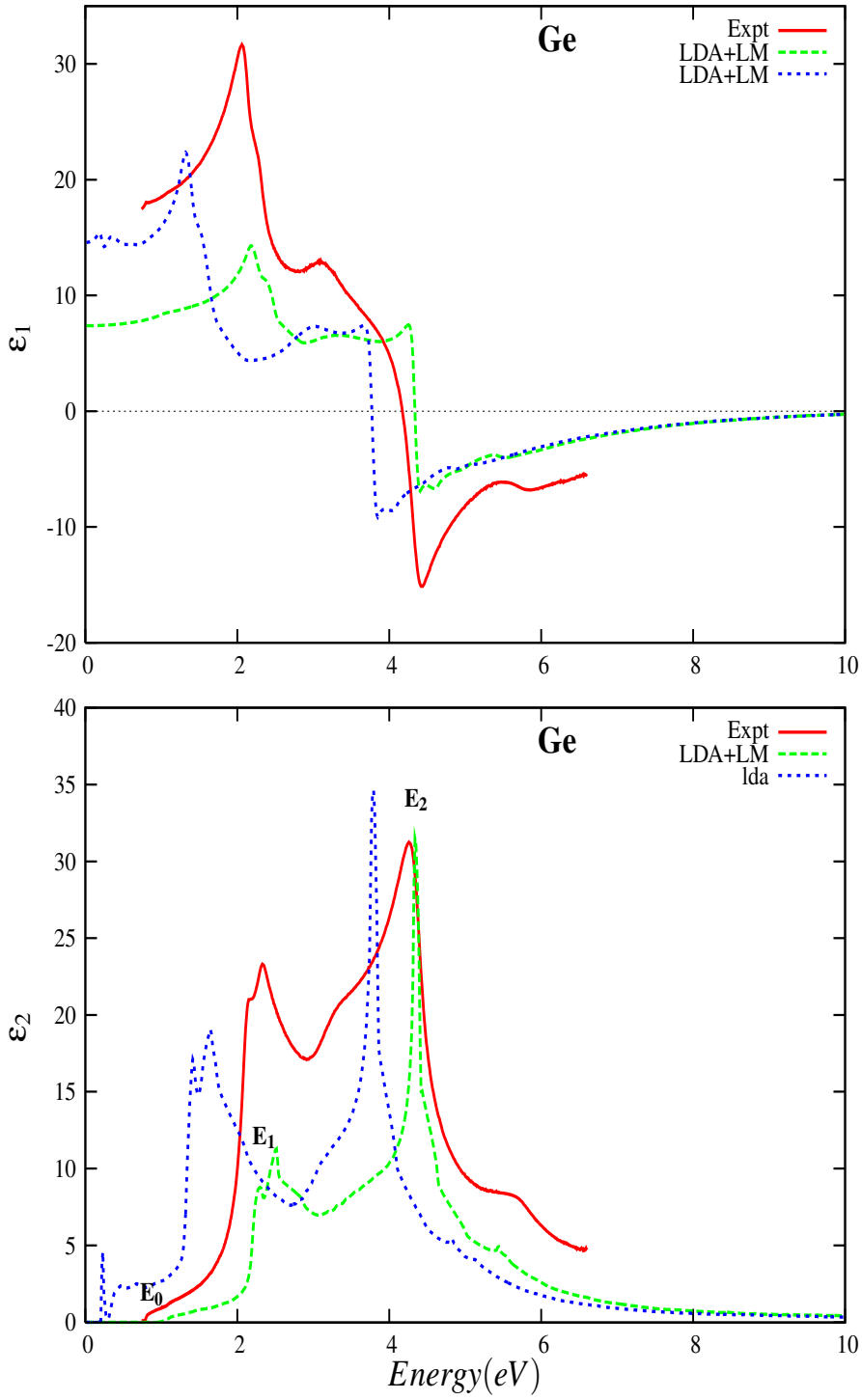

Figure 5.3: Direct Interband contribution to dielectric function of Ge and comparison with experiment. Dashes line(Blue)-LDA with LM fits, dots(green) standard LDA. Solid line(Red) are from experiment by by D'Costa *et al*, Phys. Rev. **73** 2006

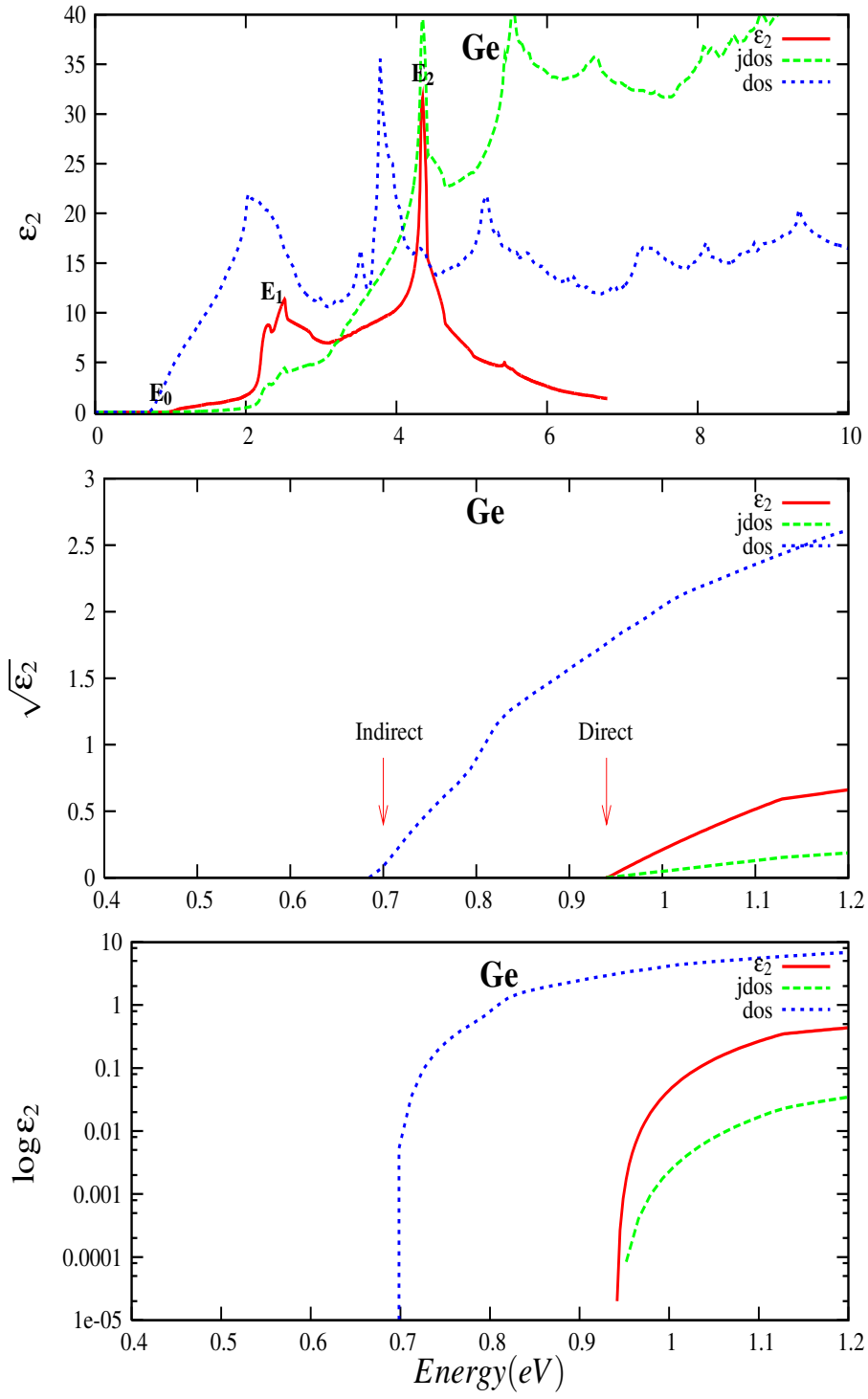

Figure 5.4: ε_2, JDOS, and DOS of Ge. The $\sqrt{\varepsilon_2}$ and the log-scale near the absorption edge help in identifyng the *direct gap*, while the edge of the DOS represent the *indirect* gap of Ge

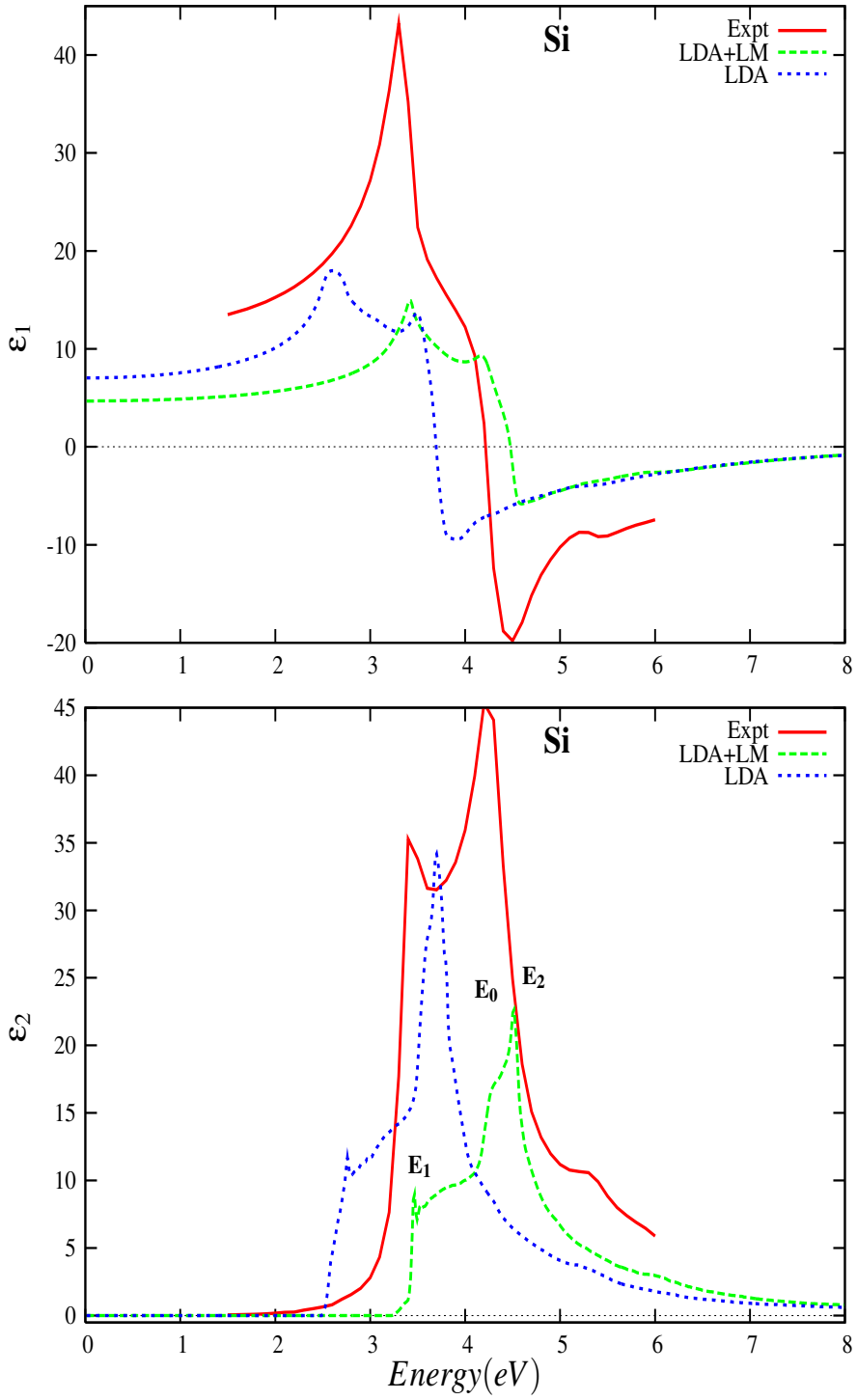

Figure 5.5: Interband contribution to dielectric function of Si and comparison with experiment. Dashes line (Blue)- LDA with LM fits, the dots(green) standard LDA and Solid line(Red) are from experiment by Aspnes *et al*, Phys. Rev. **27** 1982

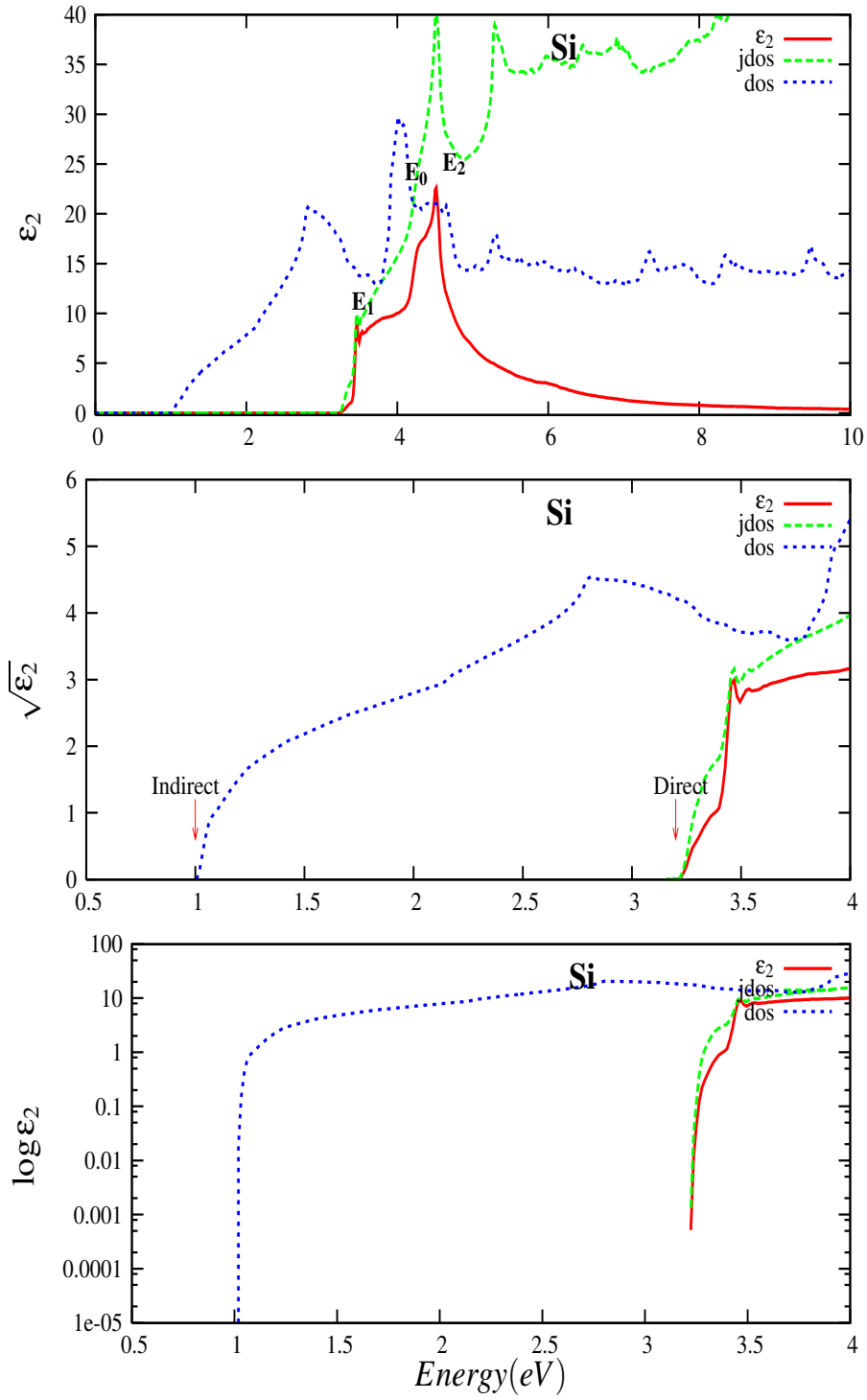

Figure 5.6: ε_2,JDOS, and DOS of Ge. The $\sqrt{\varepsilon_2}$ and the Log-scale near the absorption edge help in identifying the *direct gap*, while the edge of the DOS represent the *indirect* gap of Si

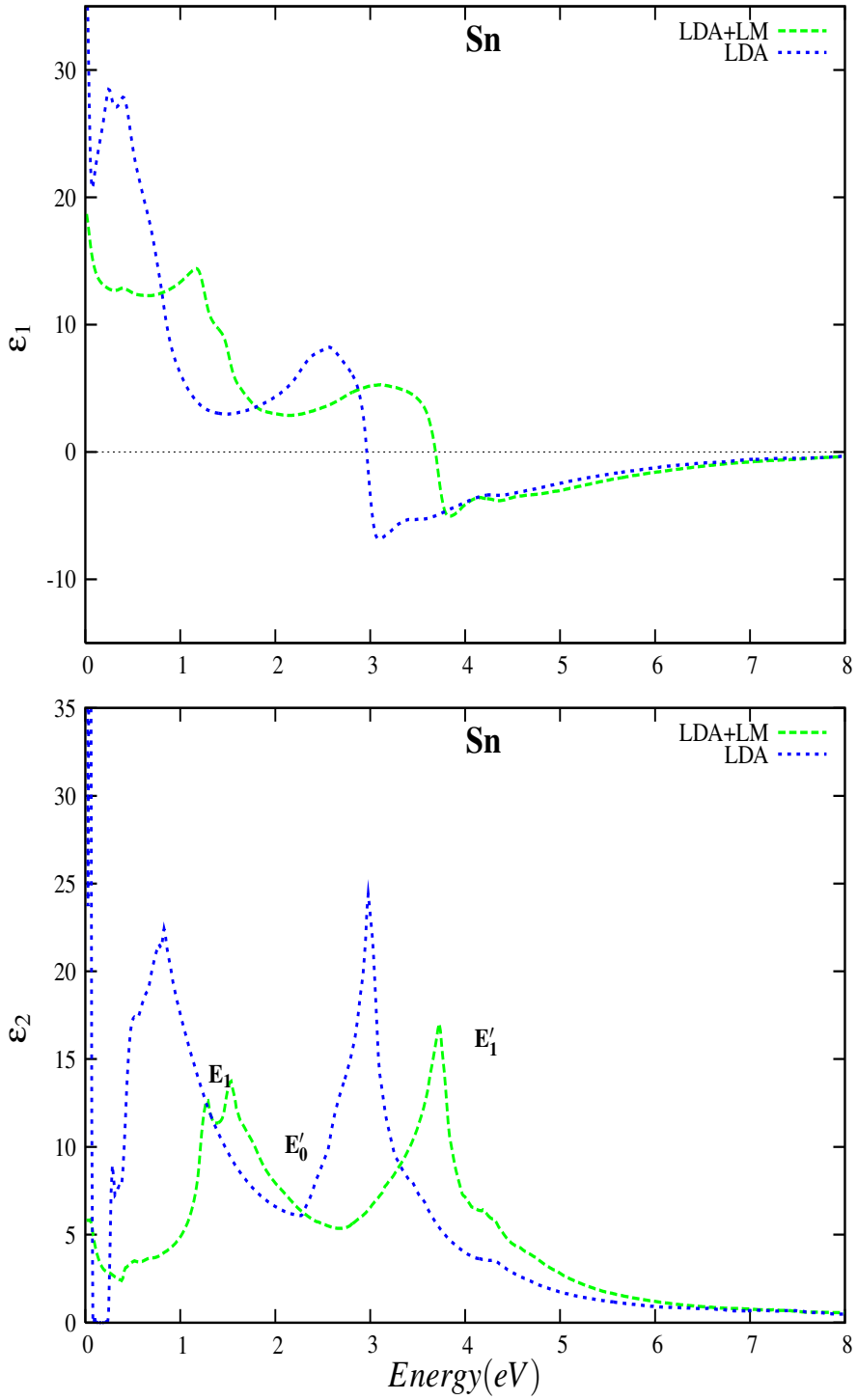

Figure 5.7: Interband contribution to dielectric function of Sn. Dashes(Blue)-LDA with LM fits, dots(green)-standard LDA

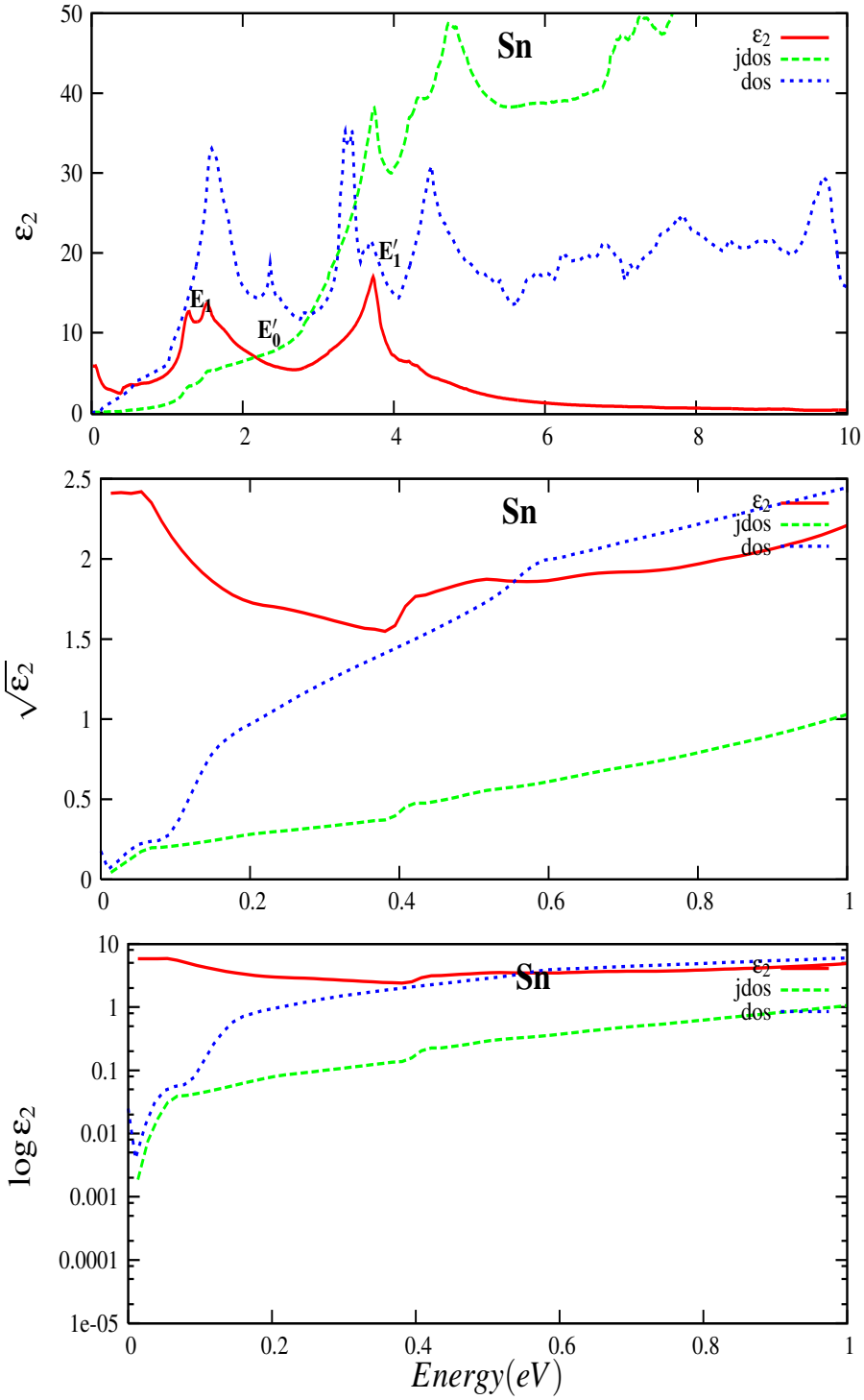

Figure 5.8: Interband contribution to dielectric function of Sn with JDOS and DOS

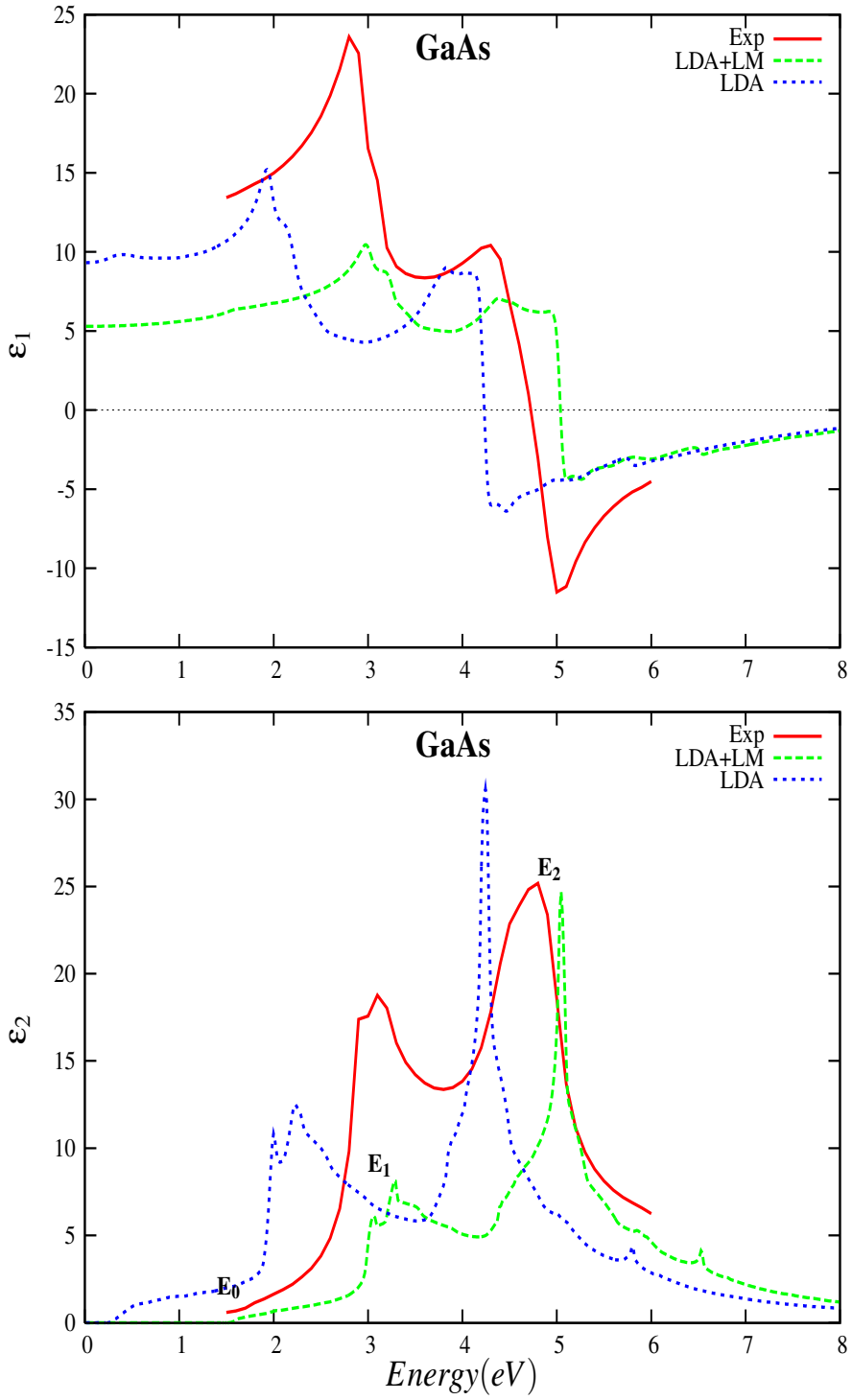

Figure 5.9: Interband contribution to dielectric function of GaAs and comparison with experiment. Dashes line (Blue)- LDA with LM fits, the dots(green) standard LDA. by Aspnes *et al*, Phys. Rev. **27** 1982

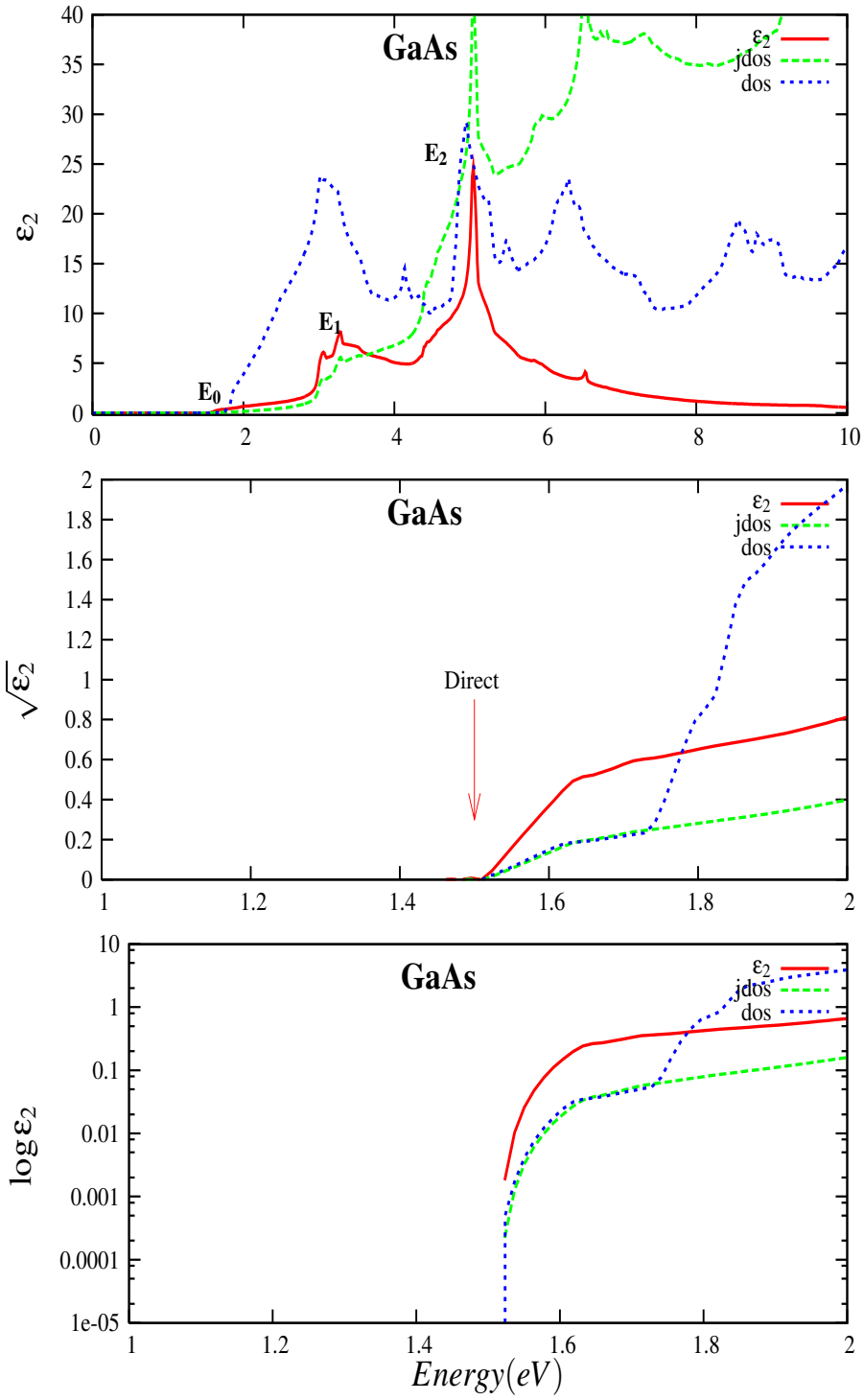

Figure 5.10: ε_2, JDOS, and DOS of Ge. The $\sqrt{\varepsilon_2}$ and the Log-scale near the absorption edge help in identifying the *direct gap*, while the edge of the DOS represent the *indirect* gap of GaAs

Chapter 6

The effect of alloying on electronic and optical properties of semiconductors

6.1 Alloys Model: Special Quasi-Random Structures (SQS)

Semiconductors alloying provides an effective way of tuning the properties of materials. This important class of material has been discussed expensively in many texts. A good reference is the review of Jaros [31] and the book *Semiconductor alloys* by An-Ban Chen and Arden Sher[10].

A typical alloys $A_{1-x}B_x$, with $(1-x)\%$ of atom A and $x\%$ of atom B. The energy gap (or transition) E_i of such a compound usually varies according to the relation

$$E_i(x) = E_i^A(1-x) + E_i^B(x) - b(1-x)x \tag{6.1}$$

where b is the *bowing* and represent the degree of deviation from linearity. E_A and E_B are the energies of the corresponding constituent. The lattice parameter generally obeys vergard's law

$$a(x) = a_A(1-x) + a_B(x) - b_{lat}(1-x)x \tag{6.2}$$

with very small bowing b_{lat}. The alloys where atom of type A occupies most lattice sites and atom B occupies the remaining sites are called substitutional alloys. We assume and diffraction studies confirms, that the alloys we are interest in are substitutional and form single crystals.

Alloying introduces two types of disorder: the *compositional disorder* due to the random occupation of lattice sites by different atoms and *structural disorder* stemming from atoms shifting from their original positions as they adjust to their new environment. This last form of disorder is smaller for closely lattice-matched materials such Si-Ge, but larger for highly mismatched alloys (HMA) such as Ge-Sn or Si-Sn. We shall show that the two types of disorder mentioned, need to be included in any accurate theoretical model. Structural disorder also breaks down the crystal symmetry. As a

result, the wave vector, **k** is no longer a good quantum number and the Bloch's theorem no longer applies. Surprisingly, the features of the optical spectra resemble those of the bulk constituent which are periodic. This suggest that experimental results are obtained by the averaging over all the possible configurations of the system. Most alloys models are based on an approximation of the averaging step. Two such models are the Virtual Crystal Approximation (VCA) and the Coherent Potential Approximation (CPA). Ultimately, the validity of a model is determined by how well its predictions agrees with experiment. For lattice-matched alloys, the commonly used method is the VCA [31]. In the VCA, atomic sites are occupied by fictitious atoms whose potential parameters are the average of the alloy constituent potentials. This very simple model has been successful in predicting the bowing of Si-Ge alloys [43], but less successful for Ge-Sn [32]. The Failure of the VCA to predict the properties of HMA stresses the importance of including substitutional and structural disorder effects. The CPA represents such an attempt. In this model, one uses the average green function and perturbation techniques to include the fluctuation in the alloy potential. Its success has been limited to closely matched alloys, but not for HMA. A review of the CPA can be found in [10]

For HMA, one needs a representation of the alloy that fully accounts for the various disorder, as well as an accurate *ab-initio* band theory suitable for large supercell. We used the TB-LMTO-ASA method with our *improved* C_{RL} and Δ_{RL} parameters.

Special Quasi-Random Structures (SQS)

For the representation of the alloy, we must select a real space configuration out of the 2^N possibilities (N i s the number of sites in binary alloy $A_{1-x}B_x$). We cannot perform direct sampling and simply perform calculations on all the possible configurations. To circumvent this difficulty, Wei and Zunger introduced the *Special Quasi-Random Structures (SQS)* [54]. These are small (N=8, 16 or 64 atoms) structures that mimic the first few but physically relevant radial correlation functions of an infinite, perfectly random

structure. Within the cluster expansion, the amount by which the property $E(\sigma = s)$ of a given structure fails to reproduce the ensemble average $\langle E \rangle$ of a perfectly random alloys is given by

$$\langle E \rangle - E(s) = \sum_{k,m} D_{k,m}[(2x-1)^k - \bar{\Pi}_{k,m}(s)]\varepsilon_{k,m} \tag{6.3}$$

where $D_{k,m}$ is the number of equivalent figures per sites and $\varepsilon_{k,m}$ the contribution of figure $\{k,m\}$ to property E [1]. $\bar{\Pi}_{k,m}(s)$ is the lattice average of the correlation function. We can see that when $\bar{\Pi}_{k,m}(s) \sim \bar{\Pi}_{k,m}(R) = (2x-1)^k$, $E(s)$ will tend to the ensemble average $\langle E \rangle$. Wei and Zunger have applied the SQS to successfully model ZB pseudo-binary alloys.

For our purpose, we developed SQS generator for Diamond Structures using Simulated Annealing. In our calculations, we use either SQS of 8, 16 or mostly of 64 (SQS-64) atoms; Convergence is usually obtained with SQS-64.

6.2 SiGe

The first alloy structure we study is the Si_xGe_{1-x} alloy. This is one of the most studied alloy and thus offer us the opportunity to test our method. We use SQS-64 for n =0, 2, 4, 6, 8 , 10, 12, 14, 16, 24, 32, 40, 48, 56, 64. All supercells were first relaxed using the FP-LMTO method. The forces after relaxation never exceeded 2 mRy/A.U. We observed from top panel of Fig. 6.1, that relaxation does play a role though small in Si_xGe_{1-x}. From the same plot and as expected, the SO splitting become important as the Ge content is increased. In the second panel, the agreement with experiment is more visible with an older experiment of Braustein *et al* [9]. There appear to be a constant small shift between our results and the more recent experiment by Alonso *et al* [53]. We attribute this discrepancy to the fact that our indirect gap for Ge differ by 0.04 eV to the experimental value. Nevertheless all the trends are present on our data.

[1] Figure $\{k,m\}$ is characterized by k, the number of atoms on its vertices and the order m of the distance separating the k atoms

In particular, the transition from L-like to X-like conduction band minimum occurs at about $x = 0.16$, in agreement with both experiments. We conclude that the new method satisfactorily interprets experimental data for alloys of Si-Ge.

6.3 GeSn

$Ge_{1-x}Sn_x$ alloys are interesting because they provide an opportunity for a direct band gap material compatible with silicon technology. Samples of this alloy system have been grown and characterized by many experimental groups [23, 36, 18]. Many theoretical studies have also been performed. Jenkins and Dow [32] used semi-empirical sp^3s^* Tight Binding combined with VCA. Bourhafs *et al* [8] use empirical pseudopotential (EPM) method with a corrected virtual crystal approximation (VCA). The first study that account for relaxation effect was by Moontragoon *et al* [42] using DFT-LDA + X-α correction. Wei *et al* [56] used SQS and EMP. Later Chibane used the Full-Potential Linearized Augmented Plane Wave (FP-LAPW) implementation of the DFT-LDA. Most of the methods cited above focused mostly on electronic properties and not a lot on optical properties. We would like to use our newly developed scheme to study both the electronic as well as the optical properties of these alloys.

As in the case of Si_xGe_{1-x}, we model the alloys with SQS-64. All our band structure calculations are done on fully relaxed supercells. We can see from Fig. 6.5 that the energy gaps are strongly affected by relaxation and also by SO (as expected since our constituent, Ge and Sn all have important SO coupling). The VCA lines illustrate the importance of fully accounting for both compositional and structural disorder.

As mentioned at the beginning of this chapter, using supercell of random alloys lead to the breakdown of symmetry and so the wave number and the critical points of the BZ loose their meaning. Yet experimental data show that the alloys still retains some characteristic of their constituent element (which are periodic crystals); therefore, it is still useful to analyze our band structure in terms of Γ, L and X symmetry point of

the BZ. An additional challenge presented by alloys, is the fact that, supercells introduce *band-folding*, thus rending the standard interpretation of energy band less obvious. Fig. 6.2 illustrates this situation. The bands in the figure are those of $Ge_{1-x}Sn_x$ with $x = 2/64$. The supercell was modeled with 2x2x2 multiples of 8-atom diamond unit cell. Because the supercell is larger than the primitive cell, the reciprocal space and the first BZ smaller. The state at the boundary of the small cell fold into the first BZ. For this reason, the bands at high symmetry points are indistinguishable.

In order to establish the nature of the state, we analyze our the bands structures with the help of both the DOS and ε_2. For example, to determine whether a band gap is direct or indirect, we compare the DOS onset with the onset of ε_2. For indirect gap, the onset of DOS occurs before that of the ε_2 [2], and for direct gap, the two onsets coincide. Fig. 6.3 illustrates this idea. We can see that as the concentration of Sn increases, the gap which starts as indirect (as in bulk Ge) progressively narrows down. The Direct gap, represented by the onset of ε_2, also become smaller; It is not obvious to exactly determine where the two crosses each other. But by carefully examining the energy bands near the band edges and the values of ε_2 near the onset, we can determine the nature of the gap. We have collected our results in Fig. 6.4. The calculated gaps are in excellent agreement with Low-Temperature (LT) results of Guevara *et al* [19] and direct gap or $E0$ energy values from D'Costa *et al* [16].

Bowing and indirect to direct gap transition

Our value for the direct gap bowing was found by fitting

$$E_D(x) = E_D^{Ge}(1-x) + E_D^{Sn}(x) - b(1-x)x \tag{6.4}$$

[2] Note that our ε_2 only contains contribution from direct transition

to the calculated gap. Our direct gap for Ge $E_D^{Ge} = 0.934$ eV and Sn direct gap of $E_D^{Sn} = -0.387eV$. We found a bowing of 3.3 eV. This value is close to the Guevara's bowing at 4 K which is 2.84 ± 0.15 eV. The small discrepancy with D'Costa bowing of 2.61 eV might due to the fact that the alloys are not truly random. Also the temperature of 15 K though low, is higher than 4 K or 0 K.

Our data also show that x_c, the critical concentration at which the gap changes from indirect to direct transition, is approximately 18 % Sn. This value is close to 17% obtained theoretically by Moontragoon *et al* [42]. This concentration is remarkably close to VCA prediction of 20%. However, at this concentration our gap is 0.17 eV whereas the VCA gap is close to ~ 0.6 eV. Experiment at room temperature finds a lower critical concentration, about 11% [23] with a gap of .44 eV. The difference between the theoretical value of x_c and the experimental value can be resolved if one takes into account the difference between the calculated indirect gap (0.70 eV) and the experimental indirect gap (0.74 eV). We observed that the vale of x_c is very sensitive to the energy gap. Therefore, the value of the crossover can only be known approximatively. Thus using the SQS and the LDA+LM method, we have been able to reproduce the experimental data for the $Ge_{1-x}Sn_x$ alloys.

Optical Spectra of GeSn

The effect of alloying on the optical spectra can be seen from Fig. 6.3. The main features of the bulk Ge spectra are retained for small Sn content. As Sn increases, the E0 peak moves closer to zero, signaling a reduction of the direct energy gap. At the same time, we observe a large broadening of the E1 peak. The presence of Sn and Ge bands combined with band-folding explain this broadening of the peaks. The E2 peak experiences a much smaller. We also note that the E1, E2 peaks are shortened and shifted to the left. The reduction in the height of the peak indicates that the coupling of the alloys states is weak. All the features observed are consistent with the optical

spectrum of D'Costa [16] obtained from ellipsometry. Our method therefore represent a additional tool for the interpretation of ellipsometric data which can be sometimes very challenging, particularly for novel materials. For example, our calculated optical spectra can help to identify features of the experimental spectra originating purely from interband transition.

6.4 SiGeSn

A new class of materials based on group IV compounds is gaining interest, these are the ternaries $Sn_xSi_yGe_{1-x-y}$. With ternary, we have an extra degree of freedom which allows for the control of both the energy band gap and the lattice parameter. We will consider the Sn-Si-Ge alloys latticed-matched to Ge. This material provides a possibility of obtaining a direct gap material that can be grown epitaxially on Ge. Using Vergard's law for ternary:

$$a(x,y) = a_{Sn}(x) + a_{Si}(y) + a_{Ge}(1-x-y) \tag{6.5}$$

and neglecting the lattice bowing, we can achieved ternary lattice-matched to Ge by keeping the ratio of Si/Sn equal to

$$y/x = \frac{a_{Sn} - a_{Ge}}{a_{Ge} - a_{si}} \sim 3.85 \text{ say } 4$$

. We have calculated the band structures and optical spectrum of few ternary latticed-matched to Germanium. The following five structures: $Sn_1Si_4Ge_{59}$, $Sn_2Si_8Ge_{54}$, $Sn_4Si_{16}Ge_{44}$, $Sn_8Si_{32}Ge_{24}$ and $Sn_{12}Si_{47}Ge5$ were considered. We show our results in Fig. 6.6. The top panel again illustrates the effect relaxation. Without relaxation the gap remains constant cross the different Sn/Si ratio. The picture changes when the systems are allowed to relax. We See in the bottom panel that the gap decreases but remains greater than the corresponding binary gap with the same Sn content; thus adding Si in Sn_xGe_{1-x} raises the gap while maintaining the lattice constant close to that of Ge.

In order to determine the nature of the gap, we resort again to optical spectra and DOS. In Fig. 6.7 we observe that for concentration of $x = 1/64$, $x = 8/64$, $x = 12/64$, the band gap is clearly indirect. For $x = 2/64$ and $x = 4/64$, DOS and the ε_2 onset are very close. But contrary to the Sn_xGe_{1-x} alloys, the exact value of the onset energy is not clear. From Fig. 6.8, we can observe that ε_2 forms a long tail beginning near the 1.5 eV, and stretching deep inside the gap. The only 2 experimental samples matching our simulation are from Kouvetakis [36]. The samples are $Sn_{.3}Si_{.13}Ge_{.83}$ and $Sn_{.08}Si_{.20}Ge_{.72}$. The first can be compared to our $Sn_2Si_8Ge_{54}$ and the second to our $Sn_4Si_{16}Ge_{44}$. The authors report a direct gap of 1.10 eV for $Sn_{.3}Si_{.13}Ge_{.83}$ and 1.04 eV for $Sn_{.08}Si_{.20}Ge_{.72}$. Based on our calculations, close to 1.1 eV, $\varepsilon_2 = 0.12$ and there are still many transitions of similar order of magnitude for energy below 1.1 eV. For example at 0.9 eV, $\varepsilon_2 = 0.033$. This suggest that ε_2 has a tail-like shape reminiscent of the urbach tail observed in amorphous materials. Another evidence of the presence of tail-states is the rapid rise of the density-of-states near the conduction band edge. A detail study of the states near the edges shall confirm the presence of such states. We can nevertheless conclude that the best candidate for direct gap are ternary with $x = 2/64$ and $x = 4/64$.

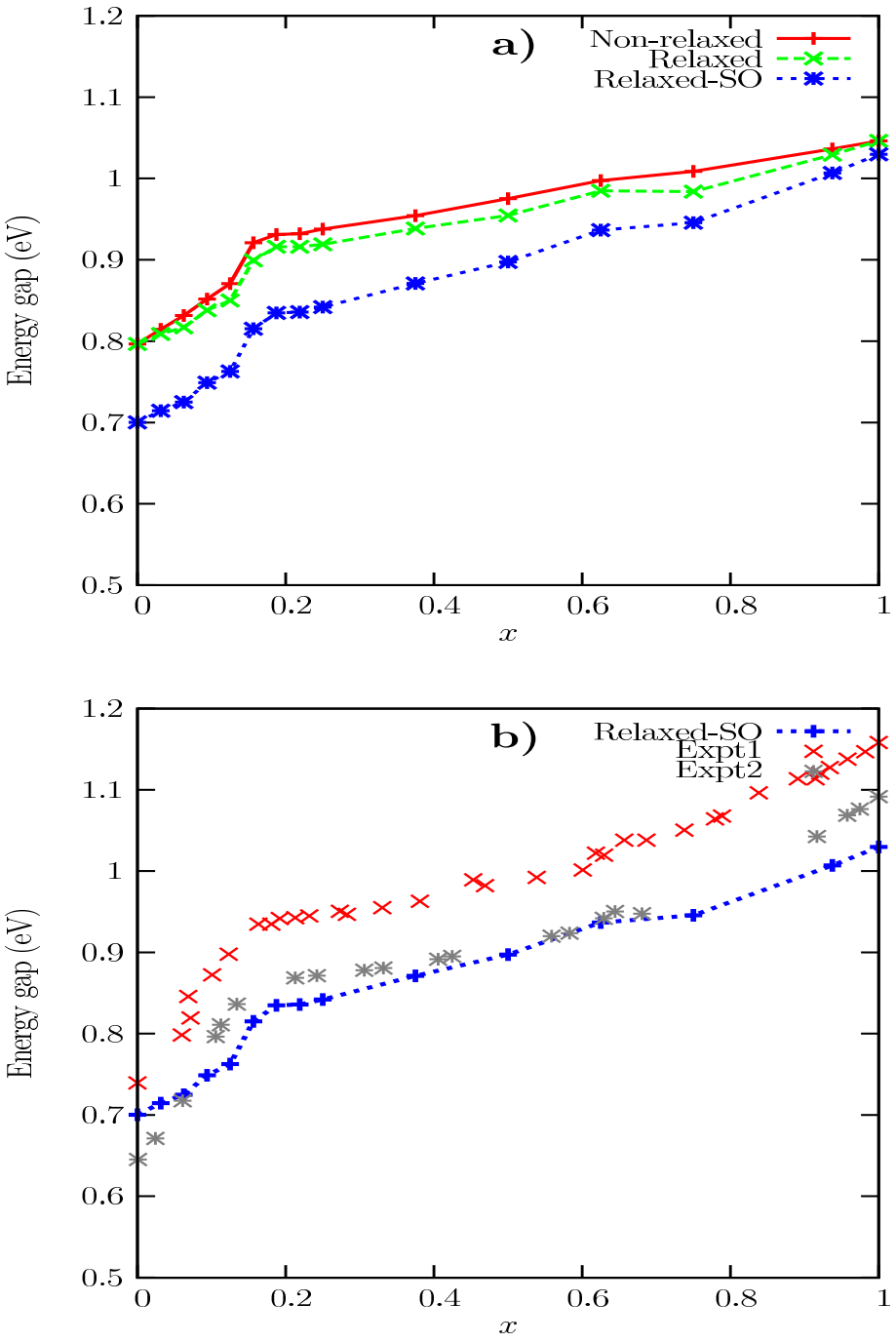

Figure 6.1: Energy gap of Si_xGe_{1-x} using the LDA+LM. a) Effect of Relaxation and Spin-Orbit (SO) splitting. b) Comparison with experiments, Expt1 is by Alonso *et al* [53] and Expt2 is by Braunstein *et al* [9].

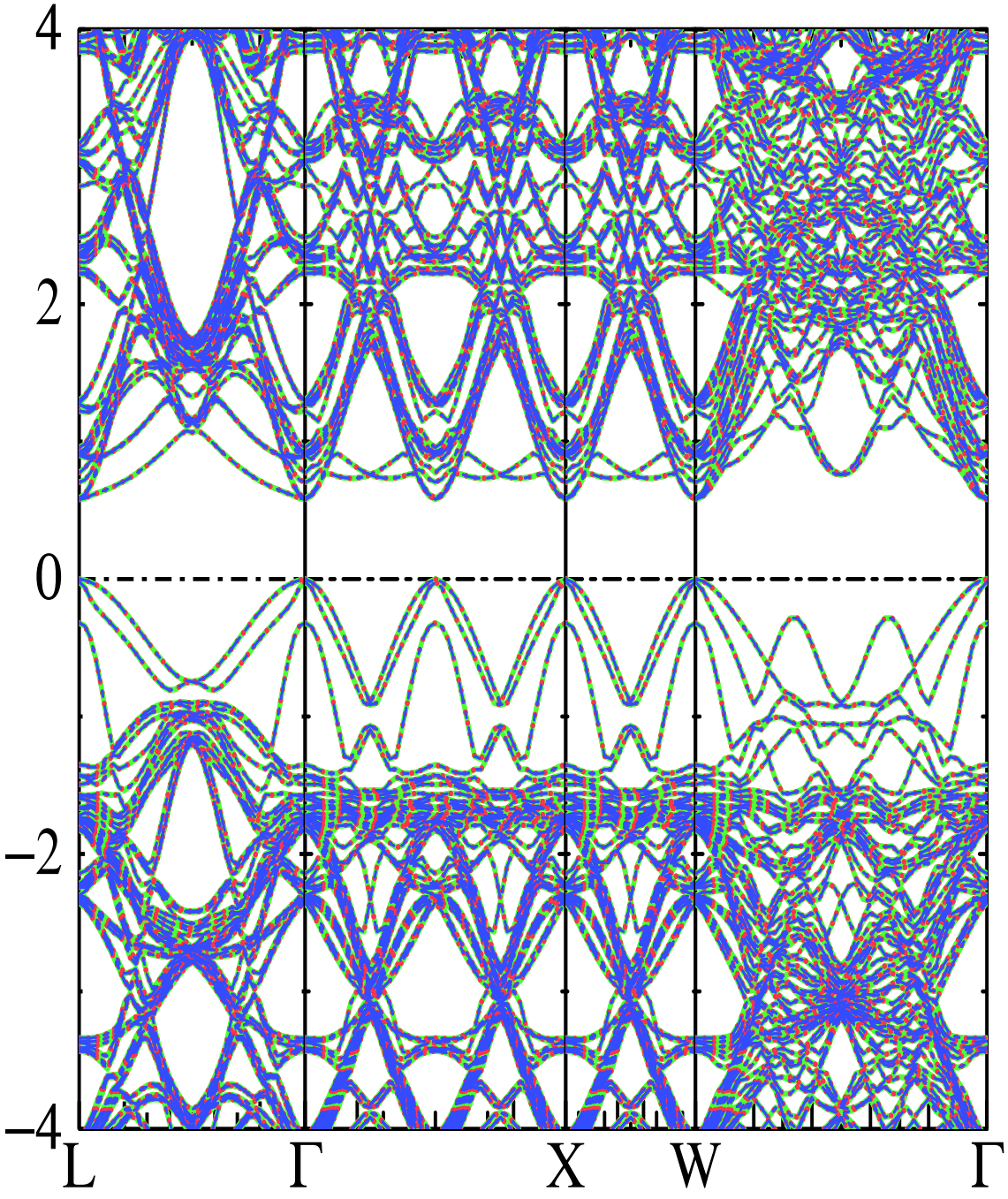

Figure 6.2: Band structure of $Ge_{1-x}Sn_x$ with $x = 2/64$ illustrating the band-folding. The bands at symmetry point Γ, L and X have almost identical shape.

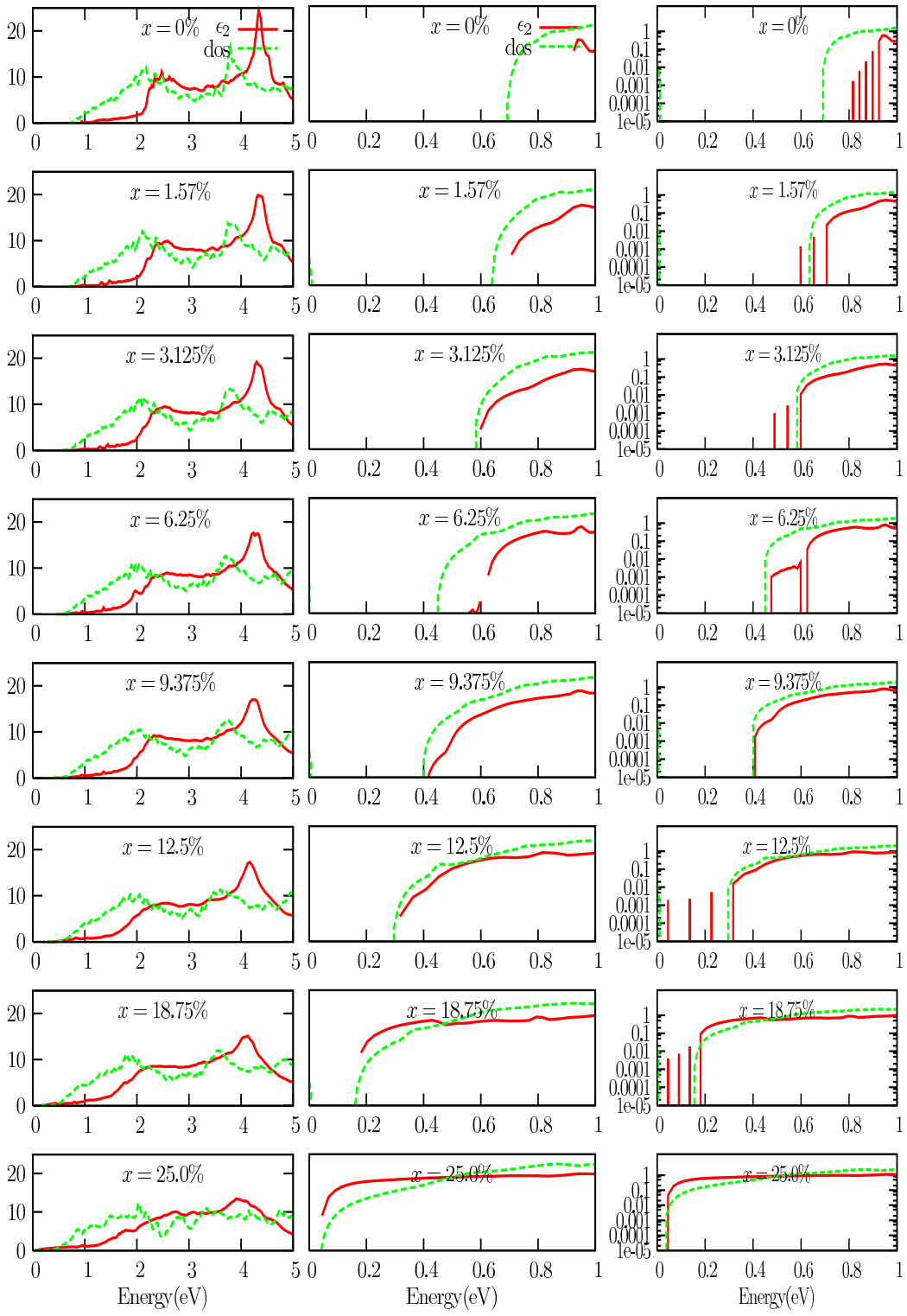

Figure 6.3: Left panel: plots of DOS and ε_2 of SQS-64 GeSn alloys. The middle panel and the right are log-scale plots of ε_2 as well as $\sqrt{\varepsilon_2}$

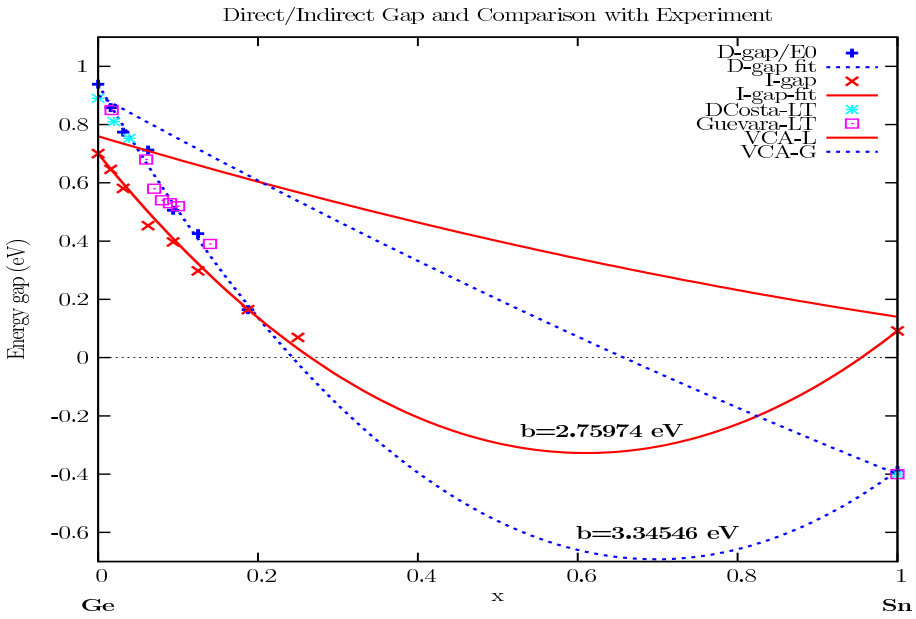

Figure 6.4: Direct and Indirect Energy-gap vs. x for $Ge_{1-x}Sn_x$. The experiment are from D'Costa [16] and Guevara [19] all at 15 and 4 K respectively. The solid (Red) line and the dotted (Blue) line represent VCA interpolation at L and Γ respectively.

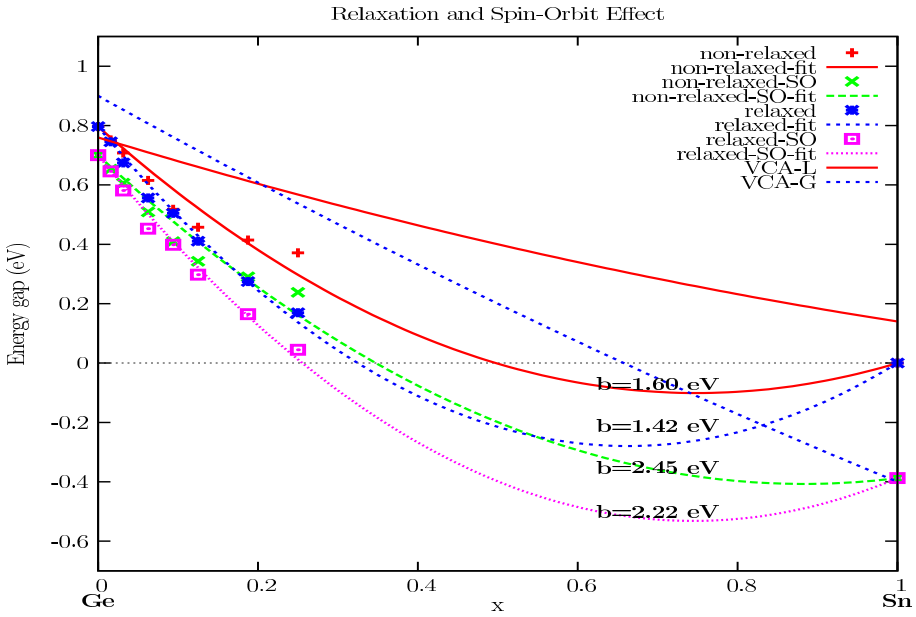

Figure 6.5: Energy-gap vs. x for $Ge_{1-x}Sn_x$ showing the effect of relaxation and Spin-Orbit coupling. Again, the solid (Red) line and the dotted (Blue) line represent VCA interpolation at L and Γ respectively

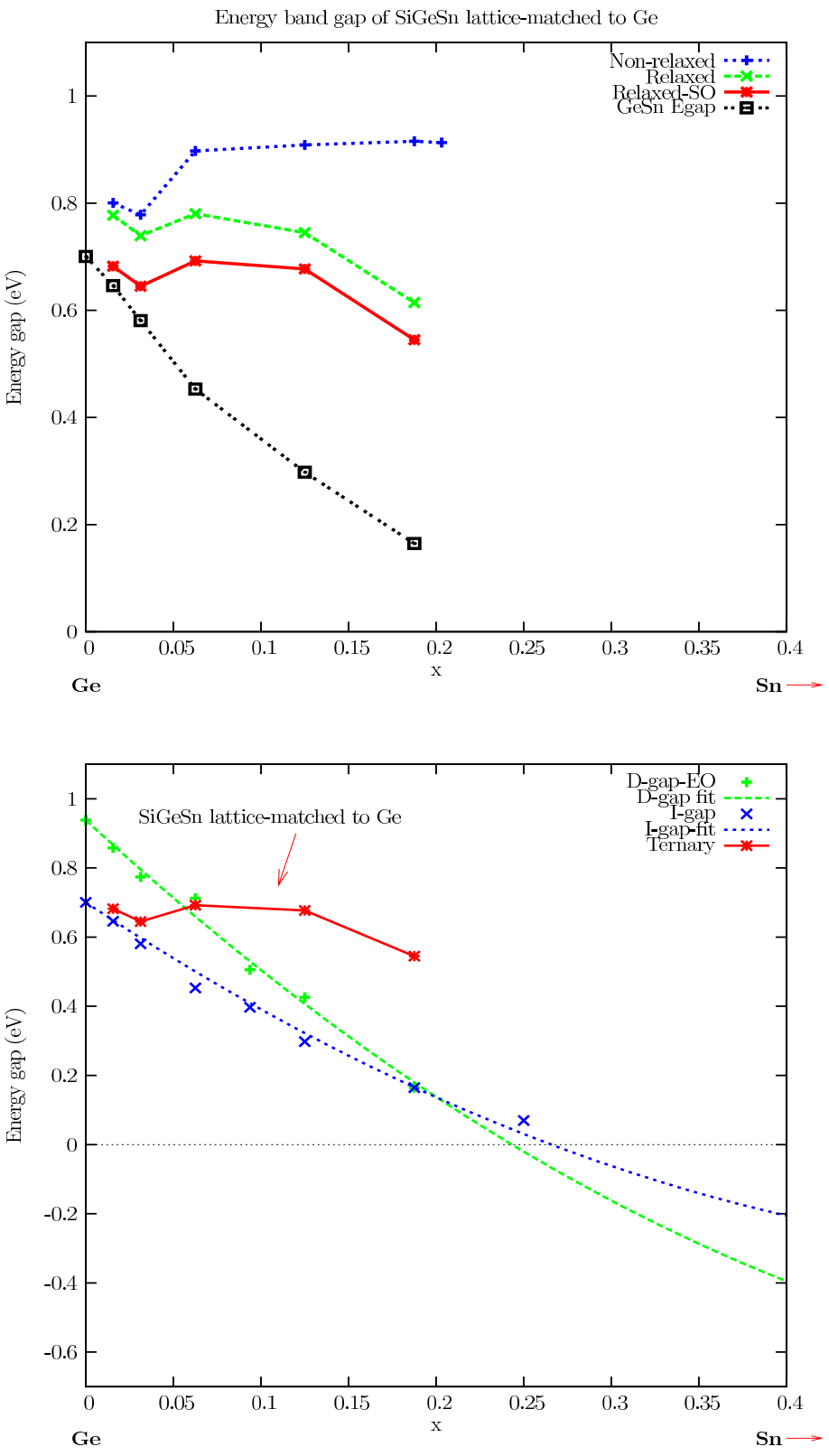

Figure 6.6: Energy gap of $Sn_xSi_yGe_{1-x-y}$ using the LDA+LM. Top) Effect of Relaxation and Spin-Orbit (SO) splitting. b) The energy gap of the ternary is compared to binary Sn_xGe_{1-x}

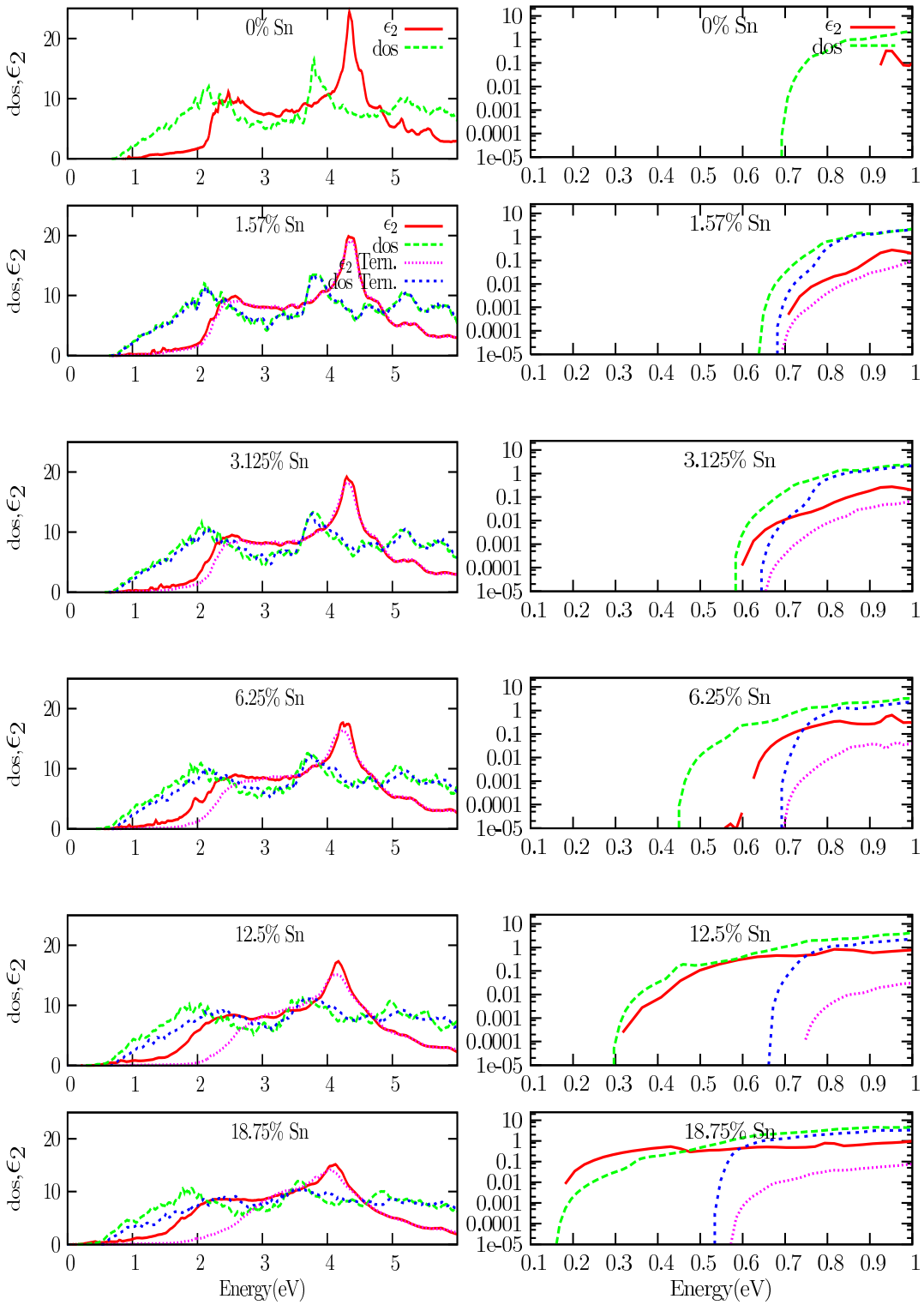

Figure 6.7: Plots of DOS and ε_2 as of function of Sn concentration in $Sn_xSi_yGe_{1-x-y}$, left panel. The right panel contains the log-scale plots of the same quantities. In (Green) and (Red) we have the binary and in (Blue) and (Pink) we have the binary

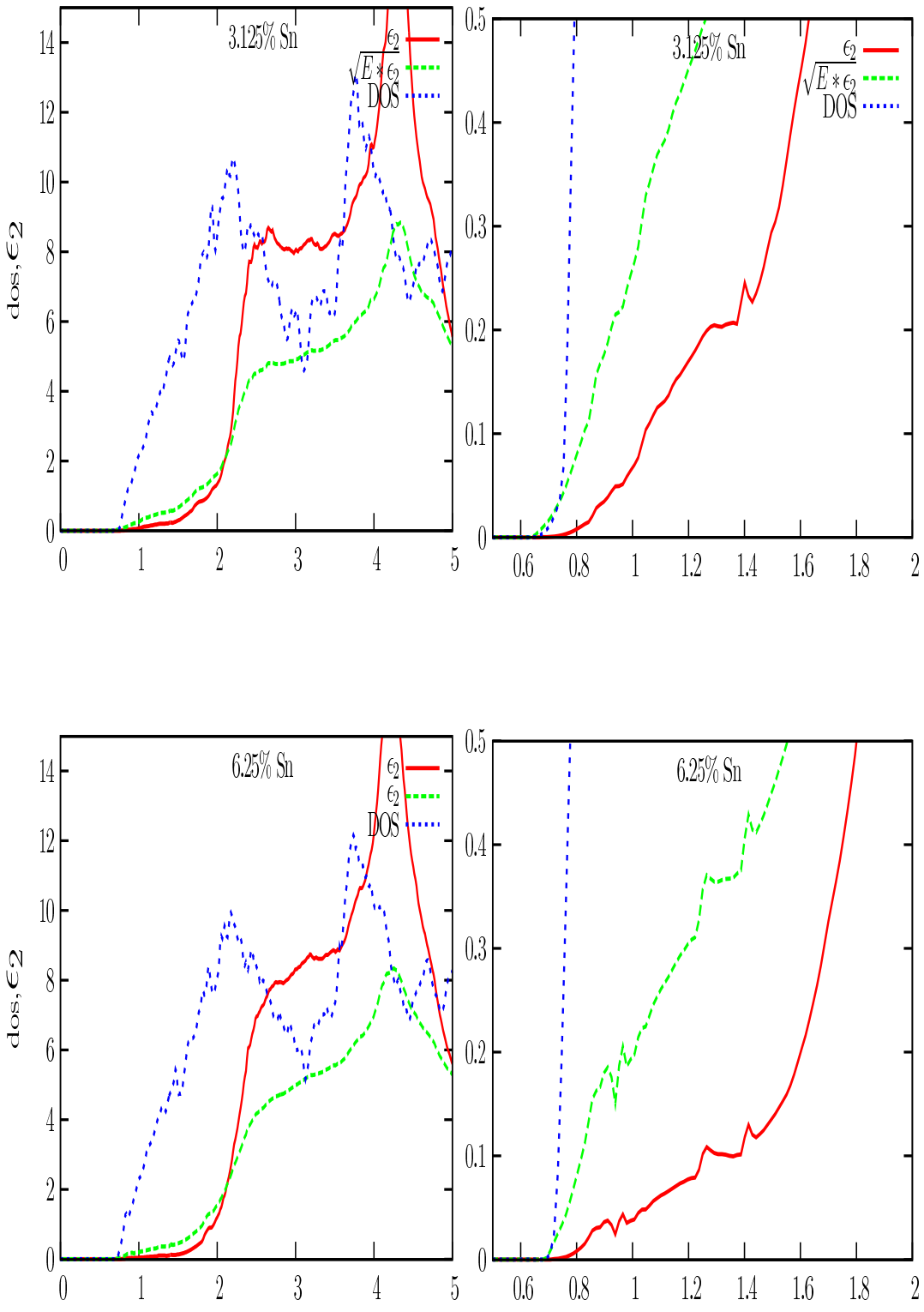

Figure 6.8: Plots of DOS and ε_2 as of function of Sn concentration in $Sn_xSi_yGe_{1-x-y}$ for x=3.125 % on the top panel and x=6.25 % on bottom panel.

Chapter 7

Summary and Future Work

In this thesis, a semi-empirical method based on the Tight-Binding Linear Muffin-Tin Orbitals (TB-LMTO) formalism and the Quasiparticle Self-consistent GW (QSGW) approximation was introduced. We began by computing the QSGW reference bands of the bulk Si, Ge and Sn. The QSGW approximation was used because it is the most reliable way to determine energy band structure. We then constructed a small and efficient hamiltonian based on the TB-LMTO method of O. K. Andersen and the Atomic Sphere Approximation (ASA). Using the Levenberg-Marquardt (LM) non-linear fit algorithm, the potential parameters, C and Δ of the hamiltonian were fitted to the QSGW reference bands. The fit were excellent in all the three semiconductors considered. The adjusted parameters were carefully tested for transferability into new environments by comparing QSGW bands structure of compounds structures such as zb-SiGe, Zb-GeSn and Zb-SiSn to bands obtained with the modified parameters (but without fitting). We also tested transferability in the case of small random alloys both binary and ternary. In all the tests, the QSGW bands and the LDA+LM bands structure agreed at least for states, up to 8 eV above the valence bands. After confirming the transferability of the parameters, we used the modified hamiltonian to generate the real and the imaginary part of the dielectric function. The dielectric functions obtained with our method was in better agreement with experiment compared to the LDA the dielectric function. All our peaks coincided with experimental dielectric function but the height of the peak was for the most part underestimated. This was expected since we did not include the local fields effects and the excitonic effects, though errors originating from the TB-LMTO-ASA were also certainly present.

We used the newly constructed hamiltonian to study the electronic band structure and

the optical properties of Si-Ge-Sn alloys. For SiGe alloys, we were able to correctly reproduce the transition from L-like band gap to X-like gap. This occurred when the Si concentration was close to 16%. For GeSn alloys, we saw that the variation of the band gaps with concentration were consistent with experiment. We obtained a direct band gap bowing of 3.33 eV which was slightly larger that LT experiment value of 2.8 eV. We think the difference might be attributed to the sample not being necessary random as assumed in the calculation. We also found a direct to indirect band gap transition near 18 % Sn close to other theoretical work. Experiment results obtained at room temperature was close to 11 %, which was slightly lower than the our calculated value of 18 %. We saw that by combining the energy bands, the DOS and ε_2, we were able to distinguish a direct to an indirect gap. This is not always obvious in supercells calculations because of band structure folding. We believe that with our method, interpretation of ellipsometric and other optical experiment of alloys and other novel material can be simplified.

We ended with a study of Si-Ge-Sn ternary structures. We focused on the structure latticed-matching Ge. This was achieved by keeping the ratio Si/Sn ratio close to 4. The five structures considered were $Sn_1Si_4Ge_{59}$, $Sn_2Si_8Ge_{54}$, $Sn_4Si_{16}Ge_{44}$, $Sn_8Si_{32}Ge_{24}$ and $Sn_{12}Si_{47}$Ge5. Only two had the potential to be direct gap material: $Sn_2Si_8Ge_{54}$ (gap -0.644 eV) and the $Sn_4Si_{16}Ge_{44}$ (gap - 0.692 eV). But experiment, put their E0 direct gap near 1.1 eV, higher than the gap from calculations. We however suspected the presence of tail states. Further study of these systems are needed to confirm this assertion.

We have achieved our set goal, developing a accurate and efficient scheme for predicting the properties of supercells. The method was used to explore direct group IV direct gap material. In future, we would like to study more ternary systems of Si-Ge-Sn; it would be interesting to study the effect of strain on these ternary. We also will like to study Ge/GeSiSn heterostructures as possible tandem material for solar cell appli-

cations. Finally, we like to test our method on other family of semiconductors such as III-V and II-VI's.

REFERENCES

[1] Stephen L. Adler. Quantum theory of the dielectric constant in real solids, *Phys. Rev.*, 126(2):413–420, Apr 1962.

[2] O. K. Andersen. Linear methods in band theory, *Phys. Rev. B*, 12:3060, 1975.

[3] O. K. Andersen and O. Jepsen. Explicit, first-principles tight-binding theory, *Phys. Rev. Lett.*, 53:2571, 1984.

[4] F Aryasetiawan and O Gunnarsson. Electronic Structure of NiO in *GW* approximation, *Phys. Rev. Lett.*, 74:3221, 1995.

[5] F Aryasetiawan and O Gunnarsson. The gw method, *Reports on Progress in Physics*, 61(3):237, 1998.

[6] N. W. Ashcroft and N. D. Mermin. *Solid State Physics*. Brooks/Cole, New York, 1976.

[7] F. Bassani and G. P. Parravicini. *Electronic States and Optical Transition in Solids*. Pergamon Press, 1975.

[8] B. Bouhafs, F. Benkabou, M. Ferhat, B. Khelifa, J.P. Dufour, and H. Aourag. Energy band structure calculation of Ge_xSn_{1-x} and Si_xSn_{1-x} alloys, *Infrared Physics amp; Technology*, 36(6):967 – 972, 1995.

[9] Rubin Braunstein, Arnold R. Moore, and Frank Herman. Intrinsic optical absorption in germanium-silicon alloys, *Phys. Rev.*, 109:695–710, Feb 1958.

[10] An-Ban Chen and Arden Sher. *Semiconductor Alloys*, Plenum Press, New York and London, 1995.

[11] Y. Chibane and M. Ferhat. Electronic structure of Sn_xGe_{1-x} alloys for small Sn compositions: Unusual structural and electronic properties, *Journal of Applied Physics*, 107(5):053512, 2010.

[12] A. V. G. Chizmeshya, M. R. Bauer, and J. Kouvetakis. Experimental and theoretical study of deviations from vegard's law in the Sn_xGe_{1-x} system, *Chemistry of Materials*, 15(13):2511–2519, 2003.

[13] Marvin. L. Cohen and James R. Chelikowsky. *Electronic Structure and Optical Properties of semiconductors*, Springer-Verlag, 1988.

[14] Gour P. Das. Introduction to linear band structure methods.

[15] V. R. D'Costa, Y.-Y. Fang, J. Tolle, J. Kouvetakis, and J. Menéndez. Tunable optical gap at a fixed lattice constant in group-iv semiconductor alloys, *Phys. Rev. Lett.*, 102(10):107403, Mar 2009.

[16] Vijay R. D'Costa, Candi S. Cook, A. G. Birdwell, Chris L. Littler, Michael Canonico, Stefan Zollner, John Kouvetakis, and José Menéndez. Optical critical points of thin-film Ge_{1-y} Sn_y alloys: A comparative $Ge_{1-y}Sny/Ge_{1-x}Si_x$ study, *Phys. Rev. B*, 73(12):125207, Mar 2006.

[17] H. Ehrenreich and M. H. Cohen. Self-consistent field approach to the many-electron problem, *Phys. Rev.*, 115(4):786–790, Aug 1959.

[18] H. Perez Ladron de Guevara, A. G. Rodriguez, H. Navarro-Contreras, and M. A. Vidal. Determination of the optical energy gap of $Ge_{1-x}Sn_x$ alloys with $0 < 0.14$, *Appl. Phys. Lett.*, 84(22):4532–4534, 2004.

[19] H. Perez Ladron de Guevara, A. G. Rodriguez, H. Navarro-Contreras, and M. A. Vidal. Nonlinear behavior of the energy gap in $Ge_{1-x}Sn_x$ alloys at 4 K, *Appl. Phys. Lett.*, 91(16):161909, 2007.

[20] G. C. Fletcher. *The Electron band Theory of Solids*. American Elsevier Publishing Company, New York, USA, 1971.

[21] David L. Greenaway and Gunther Harbeke. *Optical Properties and Bandstructure of Semiconductors*. Pergamon Press, 1968.

[22] Myrta Gruning, Andrea Marini, and Angel Rubio. Density functionals from many-body perturbation theory: The band gap for semiconductors and insulators, *The Journal of Chemical Physics*, 124(15):154108, 2006.

[23] Gang He and Harry A. Atwater. Interband transitions in sn_xge_{1-x} alloys, *Phys. Rev. Lett.*, 79:1937–1940, Sep 1997.

[24] W. A. Harrison. *The Electronic Structure*. 1st ed. W. H. Freeman and Company, San Francisco, 1980.

[25] Gang He and Harry A. Atwater. Interband transitions in Sn_xGe_{1-x} alloys, *Phys. Rev. Lett.*, 79(10):1937–1940, Sep 1997.

[26] Lars Hedin. New method for calculating the one-particle green's function with application to the electron-gas problem, *Phys. Rev.*, 139(3A):A796–A823, Aug 1965.

[27] P. Hohenberg and W. Kohn. Inhomogeneous electron gas, *Phys. Rev.*, 136(3B):B864–B871, Nov 1964.

[28] Mark S. Hybertsen and Steven G. Louie. Electron correlation in semiconductors and insulators: Band gaps and quasiparticle energies, *Phys. Rev. B*, 34(8):5390–5413, Oct 1986.

[29] J and Korringa. On the calculation of the energy of a bloch wave in a metal, *Physica*, 13(6-7):392 – 400, 1947.

[30] Jean-Marc Jancu, Reinhard Scholz, Fabio Beltram, and Franco Bassani. Empirical spds* tight-binding calculation for cubic semiconductors: General method and material parameters, *Phys. Rev. B*, 57:6493–6507, Mar 1998.

[31] M Jaros. Electronic properties of semiconductor alloy systems. *Reports on Progress in Physics*, 48(8):1091, 1985.

[32] David W. Jenkins and John D. Dow. Electronic properties of metastable Ge_xSn_{1-x} alloys, *Phys. Rev. B*, 36(15):7994–8000, Nov 1987.

[33] W. Kohn and N. Rostoker. Solution of the schrödinger equation in periodic lattices with an application to metallic lithium, *Phys. Rev.*, 94:1111–1120, Jun 1954.

[34] W. Kohn and L. J. Sham. Self-consistent equations including exchange and correlation effects, *Phys. Rev.*, 140(4A):A1133–A1138, Nov 1965.

[35] Takao Kotani, Mark van Schilfgaarde, and Sergey V. Faleev. Quasiparticle self-consistent *GW* method: A basis for the independent-particle approximation, *Phys. Rev. B*, 76(16):165106, Oct 2007.

[36] J. Kouvetakis, J. Menendez, and A.V.G. Chizmeshya. Tin-based group iv semiconductors: New platforms for opto- and microelectronics on silicon, *Annual Review of Materials Research*, 36(1):497–554, 2006.

[37] A. I. Liechtenstein, V. I. Anisimov, and J. Zaanen. Density-functional theory and strong interactions: Orbital ordering in mott-hubbard insulators, *Phys. Rev. B*, 52(8):R5467–R5470, Aug 1995.

[38] S.G. Louie and M.L. Cohen. *Conceptual foundations of materials: a standard model for ground- and excited-state properties*, Contemporary concepts of condensed matter science. Elsevier, 2006.

[39] M. Methfessel, M. van Schilfgaarde, and R. A. Casali, *A full-potential LMTO method based on smooth Hankel functions*. . in Electronic Structure and Physical Properties of Solids: The Uses of the LMTO Method, Lecture Notes in Physics, 535, edited by H. Dreysse, Springer-Verlag, Berlin (2000).

[40] Weidong Luo, Sohrab Ismail-Beigi, Marvin L. Cohen, and Steven G. Louie. Quasiparticle band structure of ZnS and ZnSe. *Phys. Rev. B*, 66:195215, Nov 2002.

[41] R. M. Martin. *Electronic Structure*. Cambridge University Press, Cambridge, UK, 2004.

[42] Pairot Moontragoon, Zoran Ikoni, and Paul Harrison. Band structure calculations of sigesn alloys: achieving direct band gap materials, *Semiconductor Science and Technology*, 22(7):742, 2007.

[43] Kathie E. Newman and John D. Dow. Theory of deep impurities in silicon-germanium alloys, *Phys. Rev. B*, 30:1929–1936, Aug 1984.

[44] Y. M. Niquet and X. Gonze. Band-gap energy in the random-phase approximation to density-functional theory, *Phys. Rev. B*, 70(24):245115, Dec 2004.

[45] W. H. Press, S. A. Teukolsky, W. T Vetterling and B. P. Flannery, *Numerical Recipes in Fortran 77*, 2nd ed., Cambridge University Press, Cambridge, 1992.

[46] J. C. Slater. The theory of complex spectra, *Phys. Rev.*, 34(10):1293–1322, Nov 1929.

[47] M. Städele, M. Moukara, J. A. Majewski, P. Vogl, and A. Görling. Exact exchange kohn-sham formalism applied to semiconductors, *Phys. Rev. B*, 59:10031–10043, Apr 1999.

[48] Shotaro Takeuchi, Yosuke Shimura, Osamu Nakatsuka, Shigeaki Zaima, Masaki Ogawa, and Akira Sakai. Growth of highly strain-relaxed $Ge_{1-x}Sn_x$/virtual Ge by a Sn precipitation controlled compositionally step-graded method, *Applied Physics Letters*, 92(23):231916, 2008.

[49] Léon Van Hove. The occurrence of singularities in the elastic frequency distribution of a crystal, *Phys. Rev.*, 89(6):1189–1193, Mar 1953.

[50] M. van Schilfgaarde, Takao Kotani, and S. Faleev. Quasiparticle self-consistent *GW* theory, *Phys. Rev. Lett.*, 96(22):226402, Jun 2006.

[51] P. Vogl, Harold P. Hjalmarson, and John D. Dow. A semi-empirical tight-binding theory of the electronic structure of semiconductors, *Journal of Physics and Chemistry of Solids*, 44(5):365 – 378, 1983.

[52] Lin-Wang Wang and Alex Zunger. Local-density-derived semiempirical pseudopotentials, *Phys. Rev. B*, 51(24):17398–17416, Jun 1995.

[53] J. Weber and M. I. Alonso. Near-band-gap photoluminescence of si-ge alloys, *Phys. Rev. B*, 40:5683–5693, Sep 1989.

[54] S.-H. Wei, L. G. Ferreira, James E. Bernard, and Alex Zunger. Electronic properties of random alloys: Special quasirandom structures, *Phys. Rev. B*, 42:9622–9649, Nov 1990.

[55] J. A. White and D. M. Bird. Implementation of gradient-corrected exchange-correlation potentials in car-parrinello total-energy calculations, *Phys. Rev. B*, 50(7):4954–4957, Aug 1994.

[56] Wan-Jian Yin, Xin-Gao Gong, and Su-Huai Wei. Origin of the unusually large band-gap bowing and the breakdown of the band-edge distribution rule in the Sn_xGe_{1-x} alloys, *Phys. Rev. B*, 78(16):161203, Oct 2008.

[57] Peter Y. Yu and Manuel Cardona. *Fundamentals of Semiconductors:physics and material properties*. Springer, 2005.